BBA - Molecular and Cell Biology of Lipids 1865 (2020) 158805

Contents lists available at ScienceDirect

BBA - Molecular and Cell Biology of Lipids

journal homepage: www.elsevier.com/locate/bbalip

An altered lipid metabolism characterizes Charcot-Marie-Tooth type 2B peripheral neuropathy

Anna Maria Giudetti[a,*,1], Flora Guerra[a,1], Serena Longo[a], Raffaella Beli[a], Roberta Romano[a], Fiore Manganelli[b], Maria Nolano[b,c], Vincenzo Mangini[d], Lucio Santoro[b], Cecilia Bucci[a,*]

[a] Department of Biological and Environmental Sciences and Technologies, University of Salento, Via Monteroni n. 165, 73100 Lecce, Italy
[b] Department of Neurosciences, Reproductive Sciences and Odontostomatology, University of Naples "Federico II", Via Sergio Pansini 5, 80131, Naples, Italy
[c] Istituti Clinici Scientifici Maugeri IRCCS, Department of Neurology of Telese Terme Institute, 82037 Telese Terme, Benevento, Italy
[d] Center for Biomolecular Nanotechnologies@UniLe, Istituto Italiano di Tecnologia, 73010 Arnesano (LE), Italy

ARTICLE INFO

Keywords:
RAB7A
Neurodegenerative disease
de novo lipogenesis
Fibroblast
Lipid droplet
Lipid metabolism

ABSTRACT

Charcot-Marie Tooth type 2B (CMT2B) is a rare inherited peripheral neuropathy caused by five missense mutations in the *RAB7A* gene, which encodes a small GTPase of the RAB family. Currently, no cure is available for this disease. In this study, we approached the disease by comparing the lipid metabolism of CMT2B-derived fibroblasts to that of healthy controls. We found that CMT2B cells showed increased monounsaturated fatty acid level and increased expression of key enzymes of monounsaturated and polyunsaturated fatty acid synthesis. Moreover, in CMT2B cells a higher expression of acetyl-CoA carboxylase (ACC) and fatty acid synthase (FAS), key enzymes of *de novo* fatty acid synthesis, with a concomitantly increased [1-^{14}C]acetate incorporation into fatty acids, was observed. The expression of diacylglycerol acyltransferase 2, a rate-limiting enzyme in triacylglycerol synthesis, as well as triacylglycerol levels were increased in CMT2B compared to control cells. In addition, as RAB7A controls lipid droplet breakdown and lipid droplet dynamics have been linked to diseases, we analyzed these organelles and showed that in CMT2B cells there is a strong accumulation of lipid droplets compared to control cells, thus reinforcing our data on abnormal lipid metabolism in CMT2B. Furthermore, we demonstrated that ACC and FAS expression levels changed upon RAB7 silencing or overexpression in HeLa cells, thus suggesting that metabolic modifications observed in CMT2B-derived fibroblasts can be, at least in part, related to RAB7 mutations.

1. Introduction

Charcot-Marie-Tooth (CMT) is a rare inherited disorder affecting the peripheral nervous system and including a variety of clinical, electrophysiological, pathological and genetic phenotypes [1–5]. It is caused by alterations in > 80 genes, among which a large number of them are involved in the regulation of membrane traffic [1–3,6–8].

The CMT type 2B (CMT2B) form is a dominant, axonal form of the disease, caused by 5 missense mutations (p.L129F, p.K157N, p.N161T/I and p.V162M) in the *RAB7A* gene, which encodes a GTPase of the RAB family [9–12]. The CMT2B peripheral neuropathy is characterized by prominent sensory loss, progressive distal weakness leading to atrophy, reduced tendon reflexes and normal or near-normal nerve conduction velocities [6,13,14]. CMT2B is also characterized by foot deformities and high frequency of ulcers and infections leading to toe and foot amputations and, for this reason, it is also classified as an ulcero-mutilating neuropathy [6,13,14]. Actually, no cure for CMT is available and physical therapy, occupational therapy, and orthopedic surgery and/or devices, represent the only possible treatment for patients.

RAB7A, hereafter referred to as RAB7, is a well-characterized ubiquitous GTPase regulating late endocytic traffic from endosomes to lysosomes and lysosome biogenesis [15,16]. RAB7 is also important for phagosome and autophagosome maturation, controlling interaction and fusion between phagosomes and autophagosomes with lysosomes and being fundamental for phagolysosome and autolysosome biogenesis [17–19]. Moreover, RAB7 has been involved in the regulation of many other processes such as apoptosis, membrane channel trafficking, and retromer recruitment and functioning [20–23]. Notably, RAB7 has also specific roles in neurons as it regulates neurotrophin trafficking and signaling, neurite outgrowth and neuronal migration during

* Corresponding authors.
E-mail addresses: anna.giudetti@unisalento.it (A.M. Giudetti), cecilia.bucci@unisalento.it (C. Bucci).
[1] These authors equally contributed to the work.

https://doi.org/10.1016/j.bbalip.2020.158805
Received 20 March 2020; Received in revised form 20 July 2020; Accepted 17 August 2020
Available online 21 August 2020

development [24–26].

Several studies have investigated the biochemical and functional properties of the CMT2B-causing RAB7 mutant proteins [27–39]. Despite the fact that several alterations have been reported, the exact mechanism by which RAB7 mutations cause the CMT2B peripheral neuropathy is still not clear.

In previous work, we demonstrated a compromised autophagic flux in CMT2B patient's fibroblasts and suggested that the altered autophagy could cause axonal degeneration leading to the neuropathy [32]. Notably, in recent years a number of reports have demonstrated a close relationship between autophagy and cellular lipid metabolism [40–43]. In particular, the involvement of autophagy in the mobilization of stored fat in the form of lipid droplets (LDs) has been reported [44] and RAB7 is a conserved component of LD membrane and it participates in LD breakdown [45–48]. In fact, RAB7 controls lipid metabolic signaling and is a central regulator of lipophagy [46,49,50].

In the nervous system, lipids accomplish a great number of key functions, from synaptogenesis to impulse conduction, and for this reason alterations in lipid synthesis and functions often induce neurodegeneration [51]. Interestingly, in some neurodegenerative diseases, lipid alterations correlate with endosomal malfunction, due to the critical role performed by lipids in endosomal membranes [52].

Given the above, we decided to study the lipidomic profile of human fibroblasts from CMT2B patients in order to track a characteristic lipid signature that can be associated with the neuropathy. Our study revealed profound differences in lipid metabolism and in LDs in CMT2B patient cells compared to healthy donor cells.

2. Materials and methods

2.1. Isolation of human fibroblasts and cell culture conditions

Skin fibroblasts were obtained from patients of the first identified Italian family affected by CMT2B [14,32]. Clinical history and symptoms of the CMT2B patients have been previously described [14]. Skin fibroblasts were also obtained from healthy control (HC) individuals age and sex matched. After informed consent for pathological diagnosis, residual tissue specimens were collected following a biobanking standard operating procedure [53]. To protect patient confidentiality, samples were anonymously encoded and used following protocols approved by the Azienda Ospedaliera Universitaria “Federico II” Ethics Committee (Ethical Committee Approval Protocol # 107/05). Aliquots of fresh tissue specimens were minced in small fragments ($< 1\ mm^3$), in a sterile environment and were then processed following protocols previously reported [54]. Tissue digestion and cell isolation were performed as previously described [32]. For all experiments, HC and CMT2B cells were subcultured in 100 × 20 mm Petri Dishes (BD Falcon) at a seeding density of 2×10^5 per dish and grown until 80% confluence. No significant differences were measured in the growing rate between groups (data not shown).

Fibroblasts and HeLa cells were cultured in 10 cm diameter plates at 37 °C in a humidified atmosphere of 5% CO_2. Cells were cultured in DMEM with 10% FBS (Fetal Bovine Serum) and the medium was renewed twice weekly. Where indicated, MG132 (10 μM, C2211 Sigma-Aldrich, St. Luis, Missouri, USA) was used for 4 h.

2.2. Transfection and RNA interference

RNA interference was used to silence the *RAB7A* gene. HeLa cells were transfected with control RNA (scrambled) or with RAB7 siRNA (Eurofins Genomics) as previously described [30,55,56] using Metafectene Si (Biontex, Munchen, Germany) transfection reagent following manufacter instructions. After transfection cells were incubated for 48 h before lysis. To overexpress RAB7, the pCDNA3.1-2xHA_RAB7 plasmid previously described [30] was transfected in HeLa cells using Metafectene Pro (Biontex, Munchen, Germany) transfection reagent. HeLa cells were also transfected with a plasmid encoding CMT2B-causing RAB7-V162M mutant protein [30] using Amaxa Cell Line Nucleofector Kit V (Lonza, Basel, Switzerland) as previously described [56] and incubated for 24 h before lysis.

2.3. Analysis of neutral cell lipids

Total lipids were extracted from fibroblasts by the Bligh and Dyer procedure and loaded on silica gel plates for separation by thin-layer chromatography (TLC). Plates were developed with hexane/ethyl ether/acetic acid (70/30/1; v/v/v). After development, plates were uniformly sprayed with 10% cupric sulfate in 8% aqueous phosphoric acid, allowed to dry 10 min at room temperature, and then placed into a 145 °C oven for 10 min [57]. The identification of cholesterol esters, triacylglycerols (TAG), free fatty acids and cholesterol was made by developing specific standards in the same experimental conditions. Spot intensity was measured by densitometric analysis.

Cell TAG were also measured, in the total lipid extract, using a kit from Roche (Monza, Italy) following *manufacturer's* instructions.

2.4. Oil Red-O staining of lipid droplets and quantification

For lipid droplets (LDs) visualization, cells were plated on 11 mm round glass coverslips. When cells reached a 80% confluency, they were washed extensively with PBS, fixed with 10% formalin for 5 min and then washed with 60% isopropanol for 5 min and left to completely dry. Subsequently, a 0.5% Oil Red-O/isopropyl alcohol solution was added to the cells, incubated for 20 min and then cells were washed several times with distilled water. After washing, nuclei were stained with 1 μM diamidino-2-phenylindole (DAPI) for 20 min. The coverslips were then washed and visualized by fluorescence microscopy. Images of cells from different samples were taken using the same settings. The stained cytoplasmic lipids were visualized and photographed by EVOS FL Auto Cell Imaging System (ThermoFisher) with PlanApo N 60 X/1.42 oil (Olymphus, Shinjuku, Tokyo, Japan). Quantification of LDs (number/cell, average size and integrated density) was determined through ImageJ Software (Version 1.5Oi, Bethesda, MD, USA). Measures were obtained by analyzing at least 50 cells in three independent experiments. Lastly, the stained cells were destained with isopropanol and the Absorbance of the destaining isopropanol was measured by spectrophotometry at a 510 nm wavelength.

2.5. GC–MS analysis of fatty acids

Total lipids were extracted by the Bligh and Dyer procedure. Fatty acids of complex lipids were transesterified by toluene and BF3 at 60 °C for 20 min. The methyl-fatty acids were analyzed by gas chromatography-MS (GC–MS) using an AGILENT 5977E gas chromatograph (Agilent, USA). This technique combines gas chromatography to mass spectrometry and is a widespread approach used in the analysis of lipid content [58].

Separation of compounds was performed on an Omegawax 250 column (30 m, 0.25 mm i.d., 0.25 mm film thickness, Agilent). The injections were performed in split mode. For gas chromatography, the column temperature was maintained at 50 °C for 2 min, and then increases from 4 °C/min to 220 °C and maintained for 15 min. Helium was used as a carrier gas at a constant flow rate of 1 ml/min. The mass spectrometer was operated in electron impact mode with a scan range of 26–400 *m/z*. The temperature of the MS source and quadrupole were set at 230 and 150 °C. Analyses were performed in full-scan mode. Compounds were identified by comparing the retention times of the chromatographic peaks with those of authentic standards analyzed under the same conditions. MS fragmentation patterns were compared with those of pure compounds, and mass spectrum database search was performed using the National Institute of Standards and Technology (NIST) MS 98 spectral database.

2.6. Cell lysis and Western blot analysis

To prepare protein extracts cells were lysed in RIPA buffer in presence of a cocktail of protease inhibitors. To this end, the culture medium was removed from the cell culture plate and cells were rinsed with chilled PBS (Phosphate Buffered Saline) 1×. PBS was then removed and cells were pelleted by centrifugation. Washed cellular pellet fractions were suspended in RIPA buffer. After freezing and thawing procedure, cells were centrifuged for 5 min at 10.000 rpm. Proteins were then quantified by the Bradford assay before loading. Proteins were then subjected to SDS-PAGE and electroblotting on nitrocellulose membranes, which were probed with specific primary antibodies for acetyl-CoA carboxylase (ACC; Cell Signaling, Rabbit 1:1000), fatty acid synthase (FAS; Cell Signaling, Rabbit 1:1000), stearoyl-CoA desaturase (SCD1; Abcam, mouse 1:1000), fatty acid desaturase 1 (FADS1; Santa Cruz, rabbit 1:1000), fatty acid desaturase 2 (FADS2; Santa Cruz, rabbit 1:1000), DGAT2 (Santa Cruz, mouse 1:1000), sterol regulatory element-binding protein (SREBP; Santa Cruz, Rabbit 1:1000) and β-actin (Abcam, mouse 1:25000). Immunoblots were revealed by enhanced chemiluminescence reagent (Bio-Rad, Hercules, California, USA). Images were acquired using the VersaDoc 1000 imaging system and individual band densities were integrated by Quantity One software (Bio-Rad).

2.7. Rate of total fatty acid synthesis from [1-^{14}C]acetate

The rate of total fatty acid synthesis in fibroblasts was followed by adding [1-^{14}C]acetate (1.56 mCi/mmol) to cells. The reaction was stopped, after 1 h, with 1 ml of 0.5 N NaOH. Cells were scraped off from plates and transferred to test tubes, and after addition of ethanol, samples were subjected to saponification. At the end of the saponification reaction, the suspension was acidified with 0.5 ml 7 N HCl and fatty acids were extracted three times with 4 ml of petroleum ether. After solvent evaporation, the radioactivity associated with labeled fatty acids was counted [59,60].

2.8. Confocal immunofluorescence microscopy

For immunofluorence analysis cells grown on 11 mm round glass coverslips were permeabilized, fixed and incubated with antibodies as described previously [56]. Nuclei were stained with DAPI (1 μg/μl). Fluorescence images were captured using a Zeiss LSM700 confocal laser scanning microscope (CLSM) (Zeiss, Germany) or a Leica CLSM microscope (TCS SP8; Leica, Microsystem GmbH, Mannheim, Germany) both equipped with a 63×/1.40 NA oil immersion objective. When indicated, cells were subjected to starvation for 24 h in EBSS medium (Sigma-Aldrich). Control cell were grown in full medium ("resting"). Subsequently, cells were washed in PBS and incubated with 2 μM BODIPY 493/503 (ThermoFisher) staining solution for 15 min at 37 °C. After two wash in PBS, cells were fixed, permeabilized and processed for immunofluorescence, as described previously [56]. Primary antibodies used were anti-LAMP1 (H4A3), deposited to the Developmental Studies Hybridoma Bank (University of Iowa, Iowa City, IA, USA) by J.T. August and J.E.K. Hildreth, at 1:250 dilution, anti-CD63 (Santa Cruz Biotechnology, 1:50), anti-SREBP-1 (Abcam, rabbit 1:100), anti-giantin (Abcam, mouse, 1:200), anti-HA (Santa Cruz Biotechnology, mouse 1:50). The secondary antibodies used were anti-rabbit and anti-mouse AlexaFluor568, anti-mouse AlexaFluor488 and anti-rabbit Cy5 (ThermoFisher, 1:500).

2.9. Real time PCR

The RNeasy Micro kit (Qiagen, Hilden, Germany) was used to isolate total RNA and SuperScript III Reverse Transcriptase (Invitrogen) was used to perform retrotranscription according to the manufacturer's instructions. Quantitative real-time PCR was carried out with Power SYBR Green (Applied Biosystems, Foster City, USA) using Applied Biosystems 7900HT Fast Real-time PCR System using primers previously described [60]. The relative expression level was calculated using the comparative CT method and expressed as "fold change." The relative quantification was considered significant when there was a minimum of two-fold change.

2.10. Statistical analysis

Results are expressed as means ± standard error of the mean (SEM). The comparison was made using one-way analysis of variance (ANOVA) and Tukey *post hoc* analysis. Student's *t*-test was used for comparisons between two groups. The statistical analysis was performed using Graph Pad Prism 7 (Version 7.03). Statistical significance was set at $P < 0.05$ with $^{*}p < 0.05$, $^{**}p < 0.005$, $^{***}p < 0.001$.

3. Results

3.1. Altered lipid composition in CMT2B fibroblasts

By GC–MS we analyzed the fatty acyl composition of two controls (HC) and three different CMT2B-derived fibroblasts and results were reported as mean ± SEM (Fig. 1). CMT2B cells showed a significant increase, with respect to controls in the percentage of monounsaturated fatty acids (MUFA), in particular in the form of oleic acid (C18:1) (Fig. 1). Moreover, CMT2B cells showed a significant increased percentage of arachidonic (C20:4, n-6) and eicosapentaenoic (C20:5, n-3) acids with a concomitant decreased percentage in linoleic acid (C18:2, n-6) (Fig. 1). No significant changes were instead revealed regarding the total amount of polyunsaturated fatty acids (PUFA) comparing CMT2B *vs* HC fibroblasts (Fig. 1). In addition, by TLC analysis we discovered a significantly higher percentage, with respect to the total amount of neutral lipids, of TAG (triacylglycerols) and of free fatty acids in CMT2B- compared to HC-derived fibroblasts (Fig. 2b). Moreover, measurement of the percentage of cholesterol esters and cholesterol (Fig. 2b) evidenced a higher value of cholesterol esters/cholesterol ratio in CMT2B with respect to HC patients (Fig. 2c). To confirm the increased amount of TAG in CMT2B cells, we spectrophotometrically measured, with a specific colorimetric test, the amount of these lipid species in all three CMT patients (CMT1, CMT2 and CMT3) with respect to controls (HC1 and HC2). We found that the level of TAG was significantly increased in all CMT-derived cells with respect to both controls (Fig. 2d).

3.2. Altered de novo lipogenesis and triacylglycerol synthesis in CMT2B patient fibroblasts

The first step of the *de novo* fatty acids synthesis, also known as *de novo* lipogenesis (*DN*L), is the ATP-dependent carboxylation of acetyl-CoA to form malonyl-CoA. This reaction is catalyzed by ACC, which represents the key enzyme of the fatty acid synthesis pathway [61]. Malonyl-CoA could then either be decarboxylated or undergo to the catalytic step involving the synthesis of the saturated fatty acid palmitate and this reaction is catalyzed by FAS [61] (Fig. 3a). In order to analyze the *DN*L activity of HC- and CMT2B-derived fibroblasts we evaluated, by Western blot analysis, ACC and FAS protein expressions. We found that both lipogenic proteins were more expressed in all CMT2B patients (CMT1, CMT2 and CMT3) with respect to HC (HC1 and HC2) cells (Fig. 3b). Quantification revealed that ACC and FAS enzymes were expressed, in all CMT2B cells, about 2.5 and 4 folds more than in control cells (Fig. 3c). To establish if these changes were due to altered transcriptional regulation, we did real-time experiments demonstrating that no significant variations were observed in the amount of mRNA for these two proteins (Fig. 3d) suggesting a post-transcriptional regulation.

Then, we decided to measure the lipogenic activity as the rate of

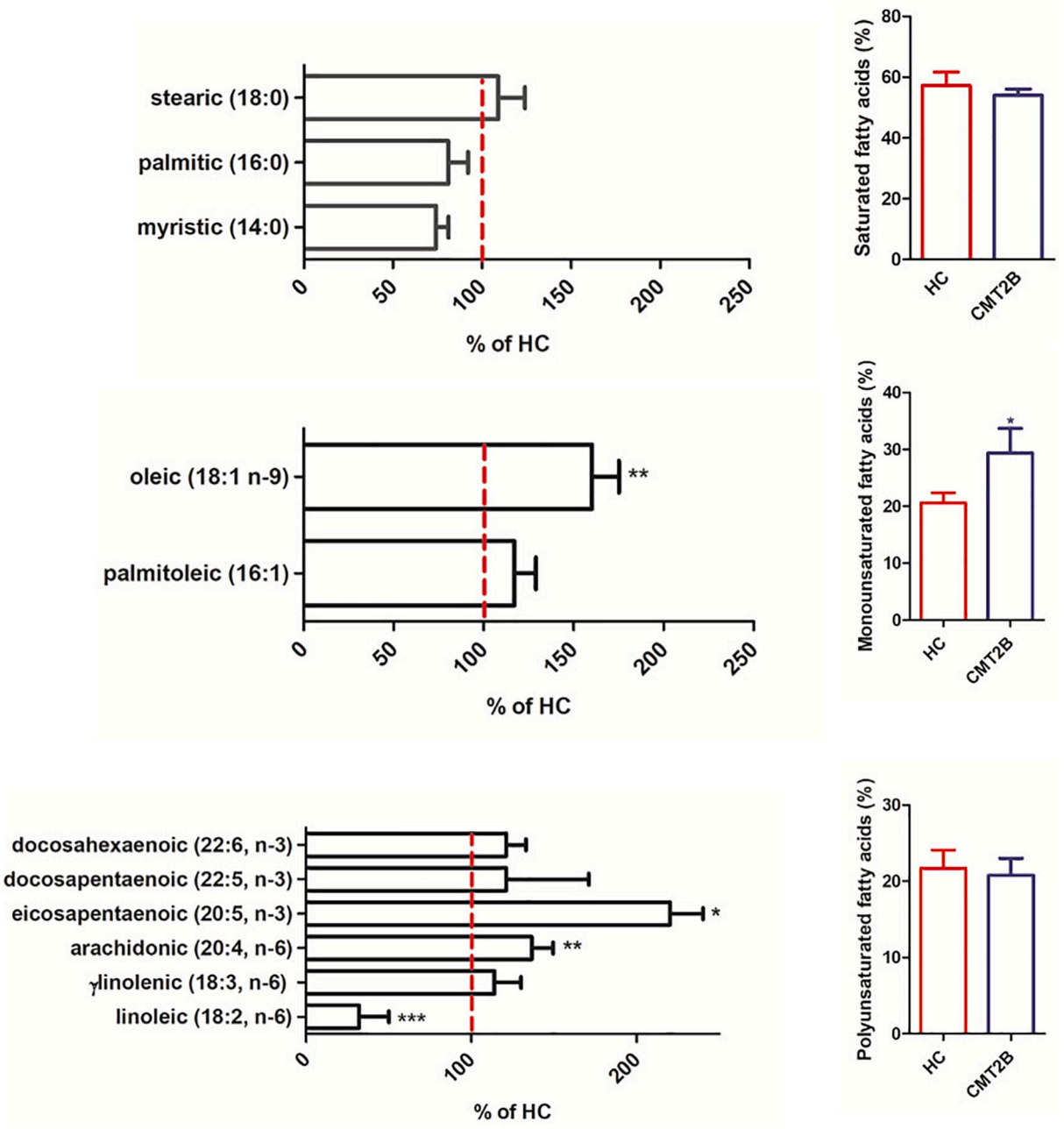

Fig. 1. Cell fatty acid composition obtained by gas chromatography-MS analysis. Total lipids were extracted from healthy control (HC) and Charcot-Marie Tooth 2B (CMT2B)-derived fibroblasts and transesterified as reported in the Material and Methods section. The analysis of fatty acid was conducted by GC–MS and values are expressed as % of the total fatty acid amount. In the figure the mean ± SEM of values obtained from three different patients and two controls, repeated three times, is reported. *P < 0.05; **P < 0.005; ***P < 0.001.

[1-^{14}C]acetate incorporation into fatty acids. Interestingly, during 1 h of incubation, CMT2B incorporated significantly more labeled precursor into fatty acids with respect to HC cells (Fig. 3e). These data correlate well with the higher expression of *DN*L enzymes measured in CMT2B with respect to control cells (Fig. 3b–c).

Cells use *de novo* synthetized fatty acids both for the synthesis of complex lipids and for the synthesis of fatty acids with a greater number of carbon atoms and/or unsaturation (Fig. 3a). In order to confirm our data, we followed the pathway of TAG synthesis by measuring the expression of DGAT2, a key enzyme in TAG synthesis. Our results revealed a higher expression, of about 2 folds, of DGAT2 in all CMT2B fibroblasts with respect to both controls (Fig. 3b).

Altogether these data indicate that *de novo* lipogenesis and TAG synthesis are more active in CMT2B compared to control cells.

3.3. CMT2B patient fibroblasts accumulated triacylglycerols as lipid droplets

To confirm our hypothesis that CMT2B fibroblasts accumulated more TAG than HC, Oil Red-O dye staining experiments were conducted. As shown in Fig. 4a, CMT2B patient fibroblasts have significantly more lipid accumulation and larger lipid droplets (LDs) compared to HC where, with this method, LDs were not visible in most cells (Supplementary Fig. 1). Moreover, a higher percentage of moderate and strong stained cells were measured in all CMT2B patient fibroblasts (CMT1, CMT2 and CMT3) with respect to controls (HC1 and HC2), where mainly cells with no or low staining were present (Fig. 4a, Supplementary Fig. 1). Quantitative analysis of LDs showed that CMT2B fibroblasts had a significant increased number of droplets/cell,

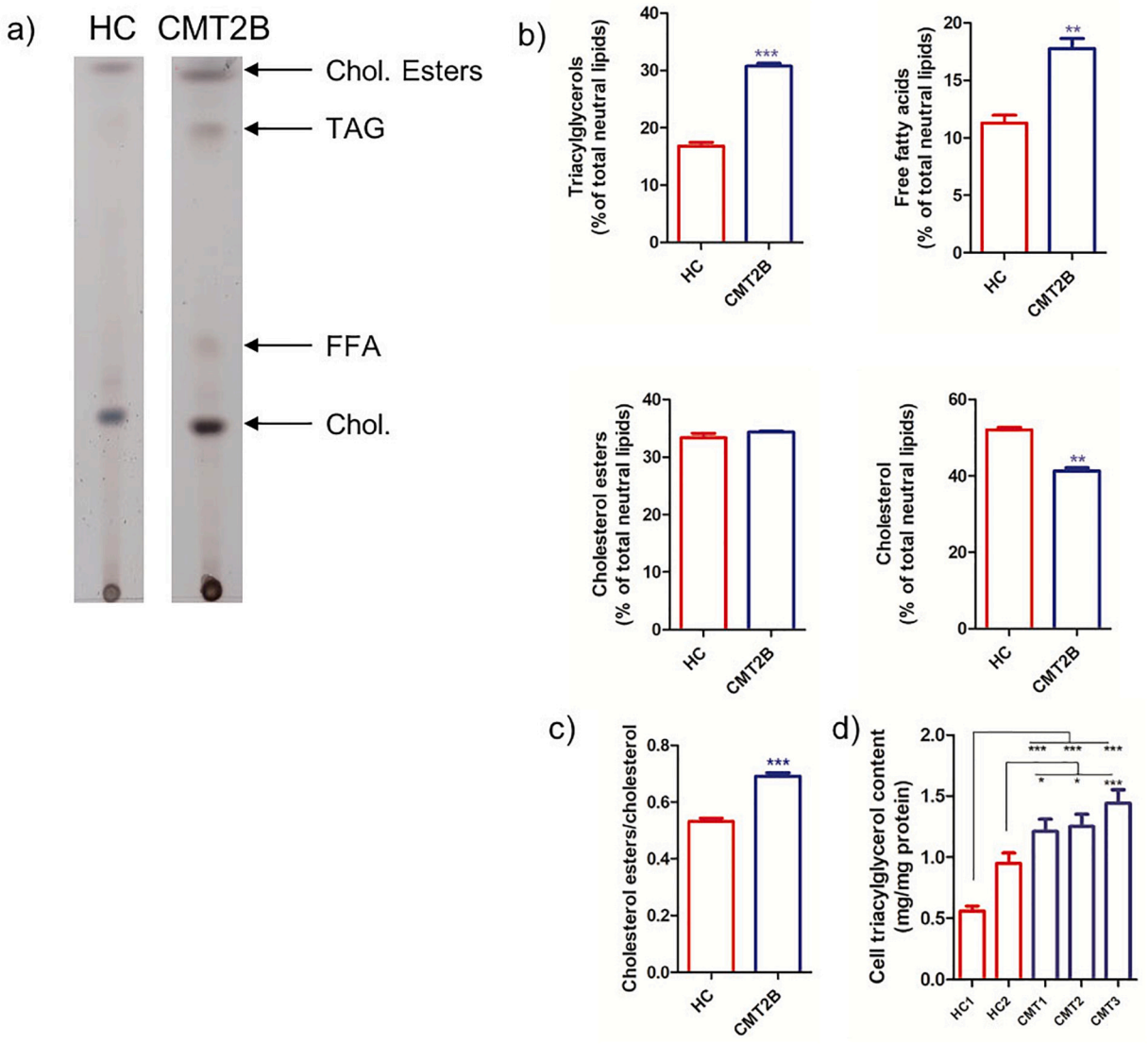

Fig. 2. Neutral lipids in HC and CMT2B fibroblasts. Total lipids from healthy control (HC)- and Charcot-Marie Tooth 2B (CMT2B)-derived fibroblasts were extracted and separated by TLC. (a) Representative TLC separation of neutral lipids from one HC and one CMT2B patient: cholesterol esters (Chol. Esters), triacylglycerols (TAG), free fatty acids (FFA) and cholesterol (Chol.). (b) Quantification of lipid amount by densitometry analysis. Different neutral lipid classes are reported as % of total neutral lipids. In the figure the mean ± SEM of values obtained from three different patients and two controls, in three independent experiments, is reported. **P < 0.005. (c) Cholesterol esters/cholesterol ratio is reported as mean ± SEM of values obtained in two HC- and three CMT2B-derived fibroblasts. s. ***P < 0.001 (d) Quantification of cell triacylglycerols from controls (HC1 and HC2) and CMT2B patients (CMT1, CMT2 and CMT3) was made spectrophotometrically by a specific kit. Values are the mean ± SEM of 4 different experiments. *P < 0.05; **P < 0.005; ***P < 0.001.

average size of droplets and of total fluorescence intensity associated with droplets (Table 1).

Subsequently, the Oil Red-O in the stained cells was eluted with isopropanol and the absorbance of the eluted sample was measured by spectrophotometry. Consistently with the morphological data, a significantly higher absorbance value was measured in the isopropanol elution of Oil Red-O staining of all CMT2B cells (CMT1, CMT2 and CMT3) than that of HC cells (medium values 0.27 ± 0.02 *vs* 0.15 ± 0.02 P < 0.05), thus indicating that CMT2B have a higher lipid content (Fig. 4b). These data indicate that CMT2B patient fibroblasts accumulate more TAG in the form of LDs compared to controls.

3.4. Pathway of fatty acid desaturations in HC- and CMT2B-derived fibroblasts

In order to better characterize CMT2B cells regarding lipid metabolism, the pathway of fatty acid desaturation was analyzed by following the expression of key enzymes of MUFA and PUFA synthesis (Fig. 5a). In particular, we followed expression of Δ-9 desaturase (SCD1), a key enzyme in the conversion of palmitate and stearate in the MUFA palmitoleate (C16:1) and oleate (C18:1). Moreover, we measured the expression of Δ-5 and Δ-6 desaturases, rate-limiting enzymes in PUFA synthesis. In all CMT2B- with respect to HC-derived fibroblasts we found a higher expression of all considered desaturases (Fig. 5b). These results well correlated with the higher expression of oleic, arachidonic and eicosapentaenoic acids measured in CMT2B- *vs* HC-derived fibroblasts (Fig. 1).

These data indicate that desaturases are more expressed in CMT2B cells compared to control cells.

3.5. Increased expression of SREBP-1 in CMT2B-derived fibroblasts

To investigate the molecular mechanism underlying the increased lipogenic activity in CMT2B cells, by Western blot analysis we measured the expression of SREBP-1, the master transcription factor regulating the expression of genes involved in fatty acid synthesis,

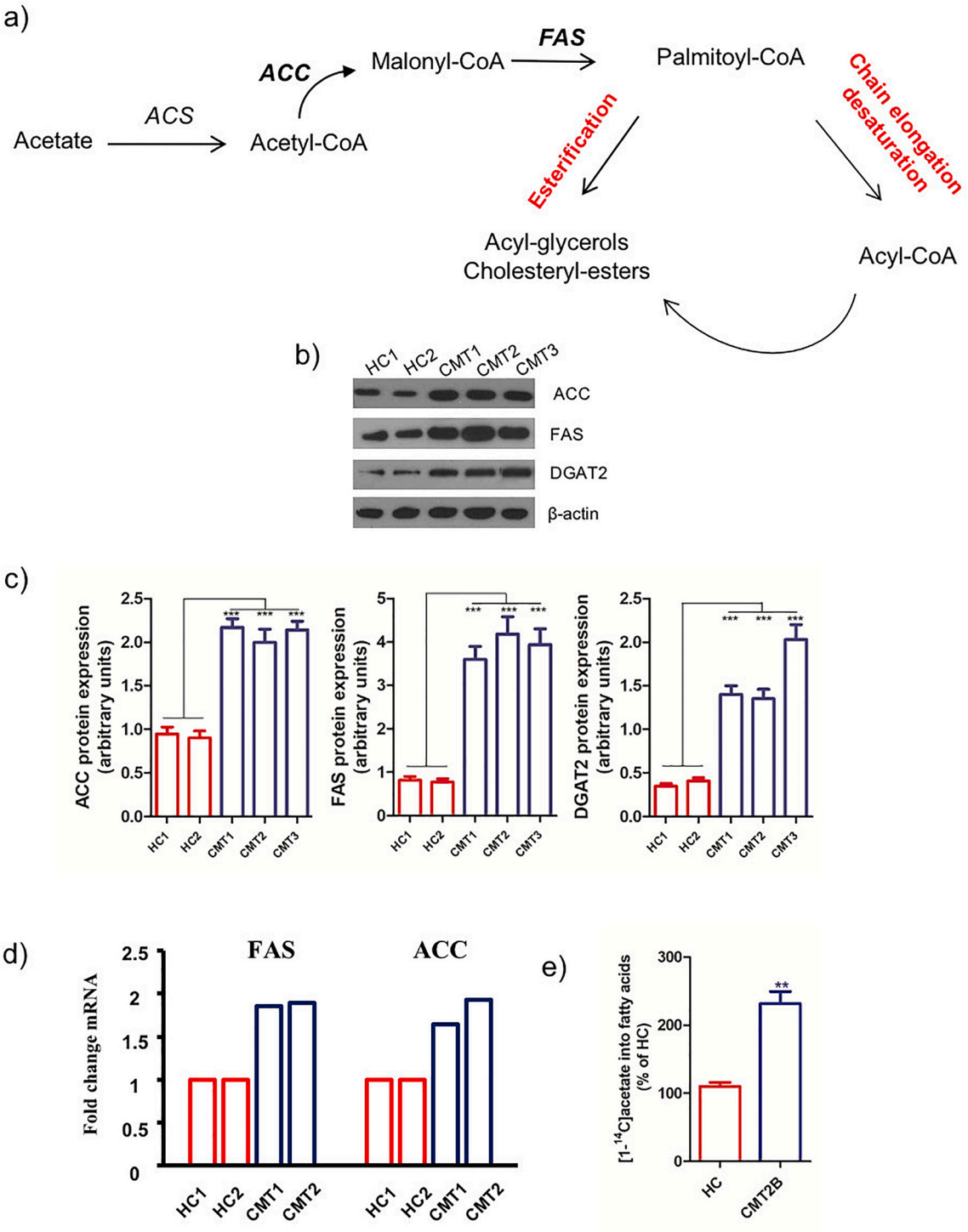

Fig. 3. Fatty acid and triacylglycerol synthesis in HC and CMT2B fibroblasts. (a) Schematic representation of the *de novo* fatty acid synthesis pathway from acetate and associated fatty acids elongation/desaturation and esterification pathways: acetate is converted into acetyl-CoA in a reaction catalyzed by acetyl-CoA synthase (ACS). Acetyl-CoA is then incorporated into malonyl-CoA in a reaction catalyzed by acetyl-CoA carboxylase (ACC) and malonyl-CoA becomes a substrate for the enzymatic complex of fatty acid synthase (FAS). The *de novo* synthetized palmitoyl-CoA can be used for esterification into complex lipids or be elongated/desaturated into fatty acids with more carbon atoms and double bonds. (b) Proteins extracted from healthy controls (HC1 and HC2) and Charcot-Marie Tooth 2B (CMT2B)-derived fibroblasts (CMT1, CMT2 and CMT3) were subjected to SDS-page electrophoresis. Membranes were analyzed by immunoblotting using specific antibodies for ACC, FAS and DGAT2. β-actin was used as the loading control. (c) Quantification of ACC, FAS and DGAT2 protein levels normalized on β-actin. The data are expressed as the mean ± SEM of three independent experiments. **P < 0.005; ***P < 0.001. (d) FAS and ACC mRNA levels were evaluated in CMT2B-derived (CMT1 and CMT2) and in control fibroblasts (HC1 and HC2) through real-time PCR. (e) The total fatty acid synthesis was measured by incubating for 1 h controls (HC1 and HC2) and CMT2B-derived fibroblasts (CMT1, CMT2 and CMT3) with [1-^{14}C]acetate. The specific activity of fatty acid synthesis is reported as the mean ± SEM of three different patients and two controls, each of which analyzed three times. Specific activity was expressed as cpm/h x mg of proteins and reported as a percentage of values measured in HC. **P < 0.005; ***P < 0.001.

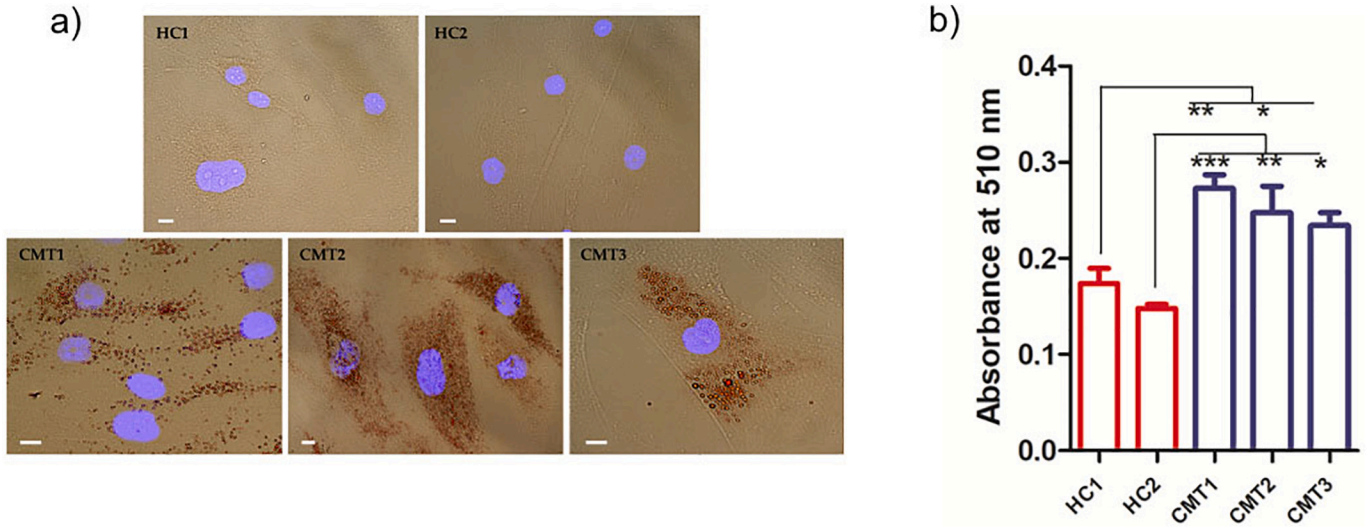

Fig. 4. Oil Red-O Staining and quantification. (a) Microscopic observations of the Oil red-O dye stained lipid droplets from controls (HC1 and HC2) and CMT2B's patients (CMT1, CMT2 and CMT3). Nuclei were labeled with diamidino-2-phenylindole (DAPI) (blue). Scale bar = 10 μm. (b) Quantification of the stained lipid droplets was performed using the eluted Oil red-O stain *via* measuring absorbance at 510 nm. Values are the mean ± SEM of 5 different experiments. *P < 0.05; **P < 0.005; ***P < 0.001.

esterification and desaturation [62]. Our data show a significant decreased expression of the precursor (pSREBP-1) forms of SREBP-1 (Fig. 6a) and a significantly higher value of the ratio between the mature (mSREBP-1) and the precursor form of SREBP-1 in all three CMT2B- with respect to HC-derived fibroblasts (Fig. 6b). These data suggest that in CMT2B, compared to HC cells, an altered expression and/or processing of this transcription factor could be responsible for the differences observed in lipid metabolism.

We have then transfected HeLa cells with a plasmid encoding CMT2B-causing RAB7 V162M mutant protein and the expression levels of mature and immature forms of SREBP-1 were analyzed. As showed in Fig. 6c and d, a decreased amount of pSREBP-1 and a significantly higher value of the mSREBP-1/pSREBP-1 ratio was present in V162M-transfected cells compared to mock transfected cells, confirming fibroblasts data. These results indicate that the RAB7 mutation is directly correlated with SREBP-1 alterations.

In order to investigate whether dysregulation of SREBP-1 level in CMT2B patients results from changes at the transcriptional level, we used real-time PCR experiments to assay the mRNA level of SREBP-1. No significant changes were observed in CMT1 and CMT2 samples compared to both controls (data not shown). Similarly, treatment with the proteasome inhibitor MG132 did not affect mSREBP-1 and pSREBP-1 levels in CMT2B cells (data not shown). Thus, to verify possible changes in SREBP-1 trafficking, we have performed immunofluorescence analysis of SREBP-1 intracellular localization using antibodies against giantin, a marker of the Golgi apparatus (Fig. 6e). In all samples SREBP-1 was predominantly localized in the nucleus and no significant differences in the intracellular distribution of this transcription factor were found among CMT2B and control cells (Fig. 6e).

Altogether these data indicate that in CMT2B cells the precursor form of SREBP-1 is less abundant suggesting an altered mechanism of regulation compared to control cells.

3.6. Modulation of RAB7 expression affects lipid metabolism

In order to establish the role of RAB7 in the regulation of lipid amount and metabolism, we decided to analyze the expression of ACC an FAS enzymes in RAB7 silenced cells. To this purpose, we transfected HeLa cells with control RNA (CTR) or RAB7 siRNA. As expected, upon siRNA treatment RAB7 expression was strongly reduced as demonstrated by Western blot analysis (Fig. 7a). Notably, silencing of RAB7 caused a reduction of both ACC and FAS protein expression (Fig. 7a and b). Conversely, we overexpressed RAB7 wt in HeLa cells (Fig. 7a) and observed a consistent and statistically significant increase of both ACC and FAS expression (Fig. 7a and c). Finally, with the aim of demonstrating the direct effect of the CMT2B-causing RAB7 V162M mutation on the differences in lipid synthesis enzymes, we expressed the RAB7 V162M mutant protein in HeLa cells (Fig. 7d) and we observed, similarly to what happens upon overexpression of RAB7 wt, a statistically significant increase of both ACC and FAS expression (Fig. 7d and e).

Altogether, these data indicate that modulation of RAB7 expression alters lipid metabolism and that lipid changes observed for CMT2B fibroblasts could be due to RAB7 alteration.

Table 1
Lipid droplet characteristics as determined by microscopy.

	N°lipid droplets/cell	Average size (μ^2)	Integrated density (pixels/μ^2)
HC1	19.3 ± 8.2	0.026 ± 0.006	6.75 ± 1.49
HC2	13.1 ± 3.21	0.037 ± 0.008	9.47 ± 2.01
CMT1	260.7 ± 16.9 (***; ***)	0.071 ± 0.004 ($^{ns;\ ns}$)	16.3 ± 1.86 ($^{ns;\ ns}$)
CMT2	450.7 ± 56.3 (***; ***)	0.096 ± 0.009 (***; ***)	24.5 ± 2.34 (***; ^{ns})
CMT3	75.9 ± 18.8 ($^{ns;\ ns}$)	0.079 ± 0.015 (**; *)	20.2 ± 3.67 (**; *)

LDs were analyzed using Image J software (Version 1.5Oi, Bethesda, MD, USA). Number per cell, average size and integrated density of LDs were determined CMT2B-derived fibroblasts (CMT1, CMT2 and CMT3) and compared to fibroblasts from healthy controls (HC1 and HC2). Results showed significant increase of three analyzed parameters in patients *versus* HC1 or HC2 (first set of asterisks *vs* HC1 and second set of asterisks *vs* HC2). Data represent the mean ± SEM of at least three independent experiments (* p ≤ 0.05; ** p ≤ 0.01 ***; p ≤ 0.001; ns = no significant).

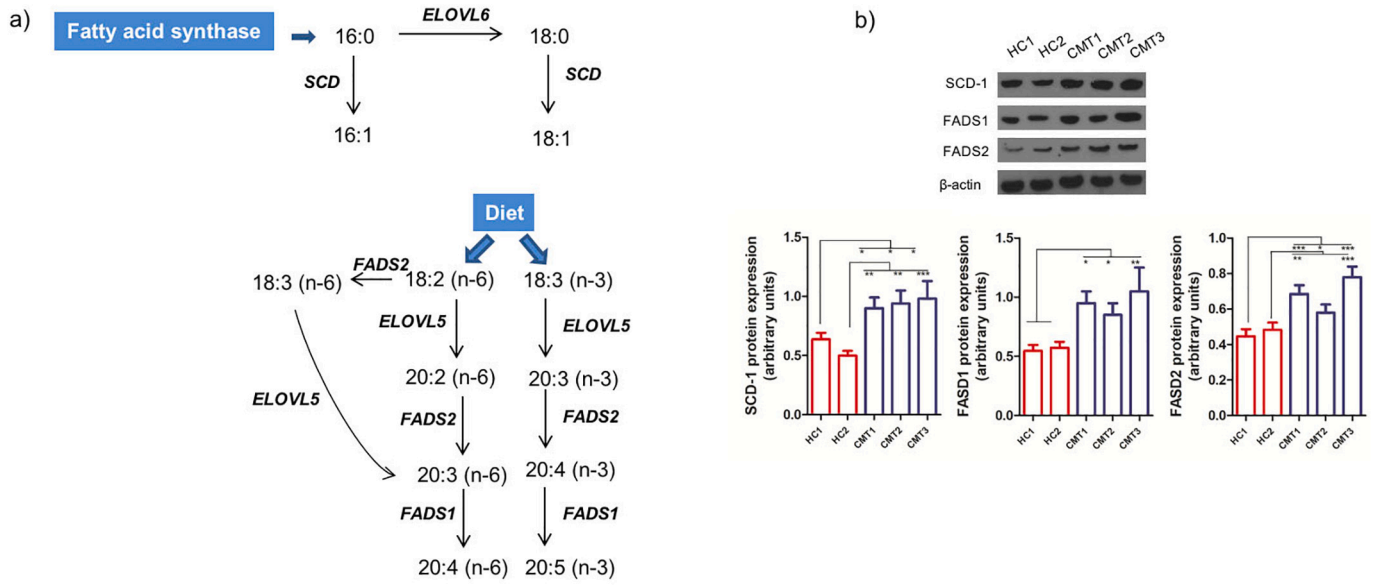

Fig. 5. Desaturase enzyme expression in HC and CMT2B fibroblasts. (a) Schematic representation of the fatty acid elongation and desaturation pathway. Palmitic acid (16:0), produced by fatty acid synthase can be both elongated by fatty acid elongase (ELOVL6) activity to stearic acid (18:0), or be converted into palmitoleic acid (16:1) by stearoyl-CoA desaturase-1 (SCD) activity. Also, stearic acid can be a substrate for SCD1 activity and be converted into oleic acid (18:1). The essential fatty acids linoleic (18:2, n-6) and linolenic (18:3, n-3) acids, introduced by the diet, are subject to ELOVL5, FADS1 and FADS2 activities to be converted into arachidonic (20:4, n-6) and eicosapentaenoic (20:5, n-3) acids, respectively. (b) Proteins extracted from healthy controls (HC1 and HC2) and Charcot-Marie Tooth 2B (CMT2B)-derived fibroblasts (CMT1, CMT2 and CMT3) were subjected to SDS-page electrophoresis. Membranes were analyzed by immunoblotting using specific antibodies for fatty acid desaturase 1 (FADS1), FADS2 and stearoyl-CoA desaturase 1 (SCD). β-actin was used as the loading control. Values are the mean ± SEM of 4 different experiments. *P < 0.05; **P < 0.005; ***P < 0.001.

3.7. Analysis of lipid droplets localization and lipophagy

In order to assess LD localization and lipophagy in CMT2B fibroblasts, also in starvation conditions, we performed immunofluorescence analysis on fibroblasts grown in full medium or incubated in EBSS buffer for 24 h. Recruitment of LDs in CD63-positive multivesicular bodies (MVBs) or in LAMP1-positive lysosomes was analyzed by staining LDs with BODIPY 493/503 [46]. As expected BODIPY-labeled LDs were present in control cells (HC1 and HC2) and were uniformly distributed in the cytosol (Figs. 8 and 9). CMT2B cells exhibited a much stronger staining revealing not only many more LDs but also LDs that were much larger and distributed predominantly at the cell periphery (Figs. 8 and 9) confirming data obtained with Oil-Red-O staining (Fig. 4a, Table 1, Supplementary Fig. 1). Furthermore, LDs exhibited physical interactions with CD63-labeled MVBs in resting (full medium) and in starved conditions in control cells, while in CMT1 and CMT2 fibroblasts, interactions between LDs and CD63-positive MVBs appeared very limited under both conditions (Fig. 8). Similarly, we observed that LAMP1-positive lysosomes surrounded LDs in control fibroblasts and these interactions increased upon starvation, while LDs present in patient's fibroblasts (CMT1 and CMT2) in both conditions were mainly not associated with LAMP1-positive structures and this was true especially for the larger LDs (Fig. 9).

In light of these observations, we expressed the RAB7 V162M mutant protein in HeLa cells and performed a similar analysis (Fig. 10). Interestingly, we observed accumulation of LDs in HeLa cells expressing the RAB7 V162M mutant protein already in resting condition. Moreover, after starvation, we observed an increase in the number and size of LDs (Fig. 10). Furthermore, very few interactions with CD63 and LAMP1 positive organelles in resting and starved conditions were observed.

All together these results demonstrate that altered breakdown of LDs observed in CMT2B cells is due to the RAB7 V162M mutation.

4. Discussion

CMT2B disease is an autosomal dominant axonal neuropathy characterized by five mutations in the RAB7A, a ubiquitously expressed GTPase controlling late endocytic trafficking. Although many studies have investigated the biochemical and functional properties of the CMT2B-causing RAB7 mutant proteins the exact mechanism by which RAB7 mutations cause a peripheral neuropathy is still unknown.

The nervous system is highly enriched in lipids that are necessary for a number of key functions, from synaptogenesis to impulse conduction, and alterations in lipid metabolism were found in a number of CMT forms. To this respect, alterations in the phosphoinositide pathway, including mutations in the phosphoinositide phosphatase MTMR2 and MTMR13/SBF2 lead to CMT4B1 and CMT4B2, respectively, and mutations in the phosphoinositide phosphatase Fig. 4, was demonstrated to induce neurodegeneration in CMT4J, impairing endolysosomal trafficking in motor neurons and Schwann cells [63–66]. Also, CMT4D is due to mutations in N-myc downstream-regulated gene 1 (NDRG1), which regulates multivesicular body formation and LDLR endosomal trafficking, thus altering lipid homeostasis and differentiation of myelinating cells [67,68]. A new missense mutation in an axonal form of CMT disease in the DGAT2 gene has been recently identified [69]. Moreover, alterations in the metabolism of cholesterol are causative of several diseases including Niemann-Pick disease, adrenoleukodistrophy and Wolman disease [70].

In the present study, we found higher expression of the *de novo* lipogenic enzymes ACC and FAS with a greater rate of labeled acetate incorporation into fatty acids in CMT2B-derived fibroblasts compared to control cells (Fig. 3). Moreover, CMT2B cells showed a higher expression of DGAT2, enzyme catalyzing TAG synthesis mainly using *de novo* synthetized fatty acids [58]. Furthermore, we also found that CMT2B fibroblasts accumulated more TAG in the form of LDs with respect to HC. On the basis of these results, we can speculate that, in CMT2B fibroblasts, *de novo* synthetized fatty acids are mainly incorporated into TAG. Accordingly, overexpression of DGAT2 in mouse

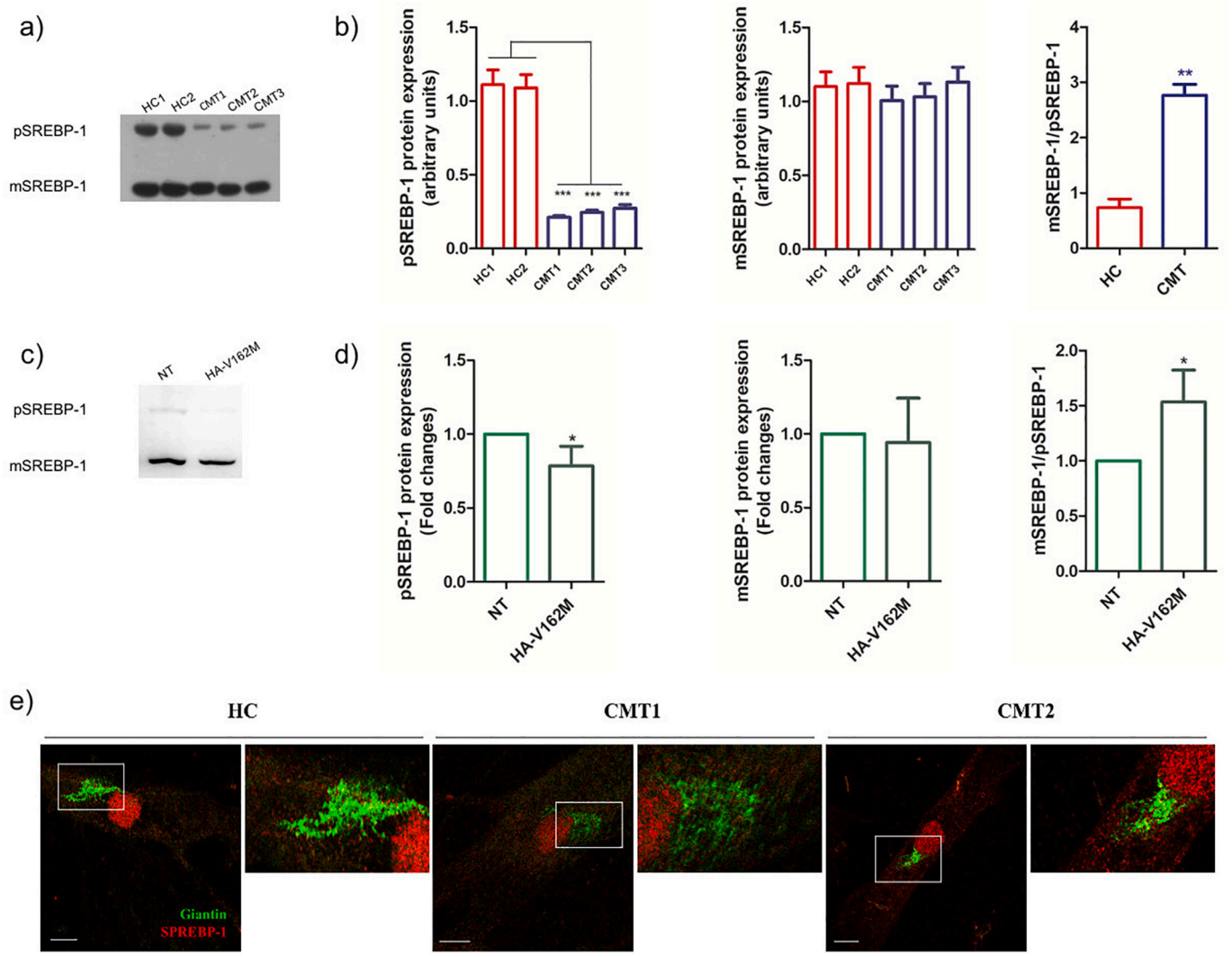

Fig. 6. SREBP-1 protein expression in HC and CMT2B fibroblasts. (a) Healthy controls (HC1 and HC2) and Charcot-Marie Tooth 2B (CMT2B)-derived fibroblasts (CMT1, CMT2 and CMT3) were lysed and protein extracts were subjected to SDS-page electrophoresis. Lysates were then analyzed by immunoblotting using a specific antibody for SREBP-1 which recognized both the precursor (pSREBP-1) and the mature (mSREBP-1) form. (b) Signals from pSREBP-1 and mSREBP-1 were quantified by densitometric analysis and the ratio between mSREBP-1 and pSREBP-1 was calculated for control and CMT2B cells, $^{**}P < 0.005$; $^{***}P < 0.001$. (c, d) In HeLa cells expressing RAB7 V162M mutant protein, pSREBP-1 and mSREBP-1 protein levels were evaluated by densitometric analysis, $^{*}P < 0.05$. (e) Intracellular localization of SREBP-1 in control and CMT2B fibroblasts was evaluated though immunofluorescence using antibodies against SREBP-1 (red) and giantin (green). Nuclei were stained with DAPI (blue). Scale bar: 10 μm.

has been demonstrated to induce accumulation of LDs in the cytosol [71].

An increased cholesterol ester/cholesterol ratio was also revealed in CMT2B-derived fibroblast compared to controls. Cholesterol esters can be stored in LDs and TAG and cholesterol esters are the two major storage neutral lipids that make up the core of LDs [72]. Thus, these results further support the increased tendency of CMT2B-derived fibroblasts to accumulate LDs compared to control cells.

LDs are specialized organelles representing the predominant form of cell TAG storage [73]. LDs can be selectively degraded by autophagy through a process termed lipophagy [47]. By this process, TAG associated with LDs are taken up by autophagosomes and then degraded by acid hydrolases [47], providing fatty acids to β-oxidation for energetics purpose [47]. Indeed, inhibition of lipophagy increases hepatic TAG and LDs both *in vitro* and *in vivo* [74] and it has been reported that a persistent blockage of autophagy in cultured hepatocytes, blasting the balance between lipogenesis and lipolysis toward the former one, leads to a significant increase in the number of LDs [44]. Moreover, it is known that in nutritional stress conditions RAB7 is the master regulator of LD-autophagic interaction and its activation is needed for initiation of LD catabolism through autophagy [46]. Considering our previous work in which we demonstrated a reduced autophagic flux in CMT2B-*vs* HC-derived fibroblasts [32], we demonstrated that CMT2B-causing RAB7 V162M mutant protein induces impairment of lipophagy and it could have a role in the observed changes in the *DNL* and in TAG accumulation. Thus, reduced lipophagy can induce the synthesis of fatty acid that, throughout an overexpression of DGAT2 can be massively transformed into TAG and accumulated into LDs. It should be noted that DGAT2 has been shown to be closely associated with LDs, also taking part in their formation [75] and to possess a C-terminal sequence necessary and sufficient for targeting DGAT2 to LDs [76].

CMT2B-derived fibroblasts showed also higher expression, compared to control cells, of SCD1, a Δ9-desaturase which converts palmitate and stearate in MUFA palmitoleate and oleate, this latter representing the major substrate for TAG synthesis [77]. SCD1 represents an important regulator of the lipogenic rate [78] and, in the liver, the pathway of *DN*L and fatty acid desaturation by SCD1 appears to be coordinately regulated [79]. The implication of SCD1 in autophagy *via*

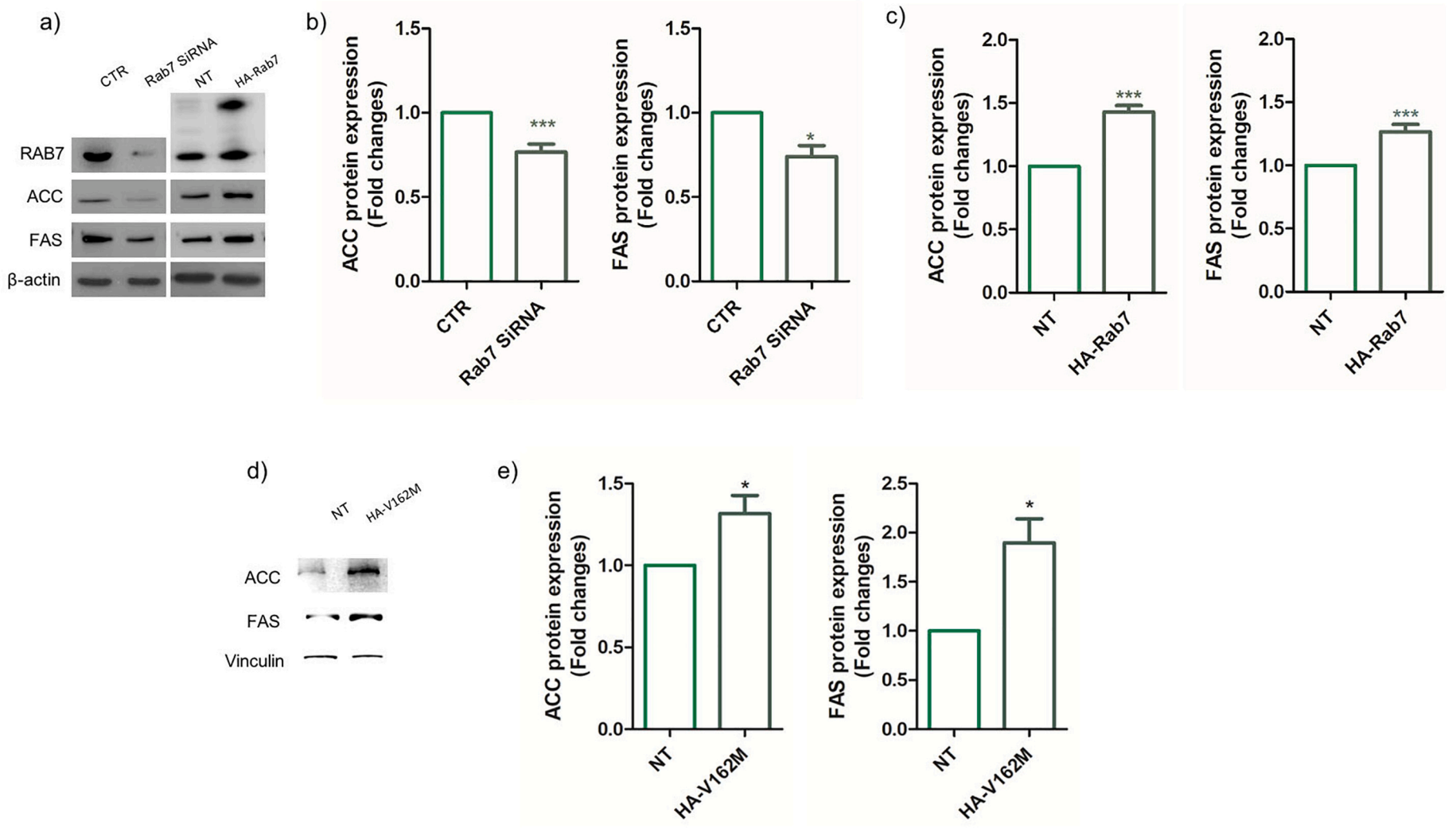

Fig. 7. Lipogenic protein expression in RAB7 silenced, RAB7 overexpressing and V162M expressing HeLa cells. (a, d) Lysates from HeLa cells transfected with control RNA (CTR), RAB7 siRNA, control plasmid (NT), plasmid for HA-tagged RAB7 overexpression (HA-RAB7) or plasmid encoding CMT2B-RAB7 V162M (HA-V162M) were subjected to SDS-PAGE and analyzed by immunoblotting using specific antibodies for acetyl-CoA carboxylase (ACC) and fatty acid synthase (FAS). Antibodies again β-actin were used as loading control while antibodies against RAB7 were used to check RAB7 silencing and overexpression. (b, c, e) Signal intensity was quantified by densitometric analysis and reported as fold changes of RAB7 SiRNA, HA-RAB7 and HA-V162M samples compared to their controls. Values are the mean ± SEM of three different experiments. *P < 0.05 **P < 0.01 ***P < 0.001.

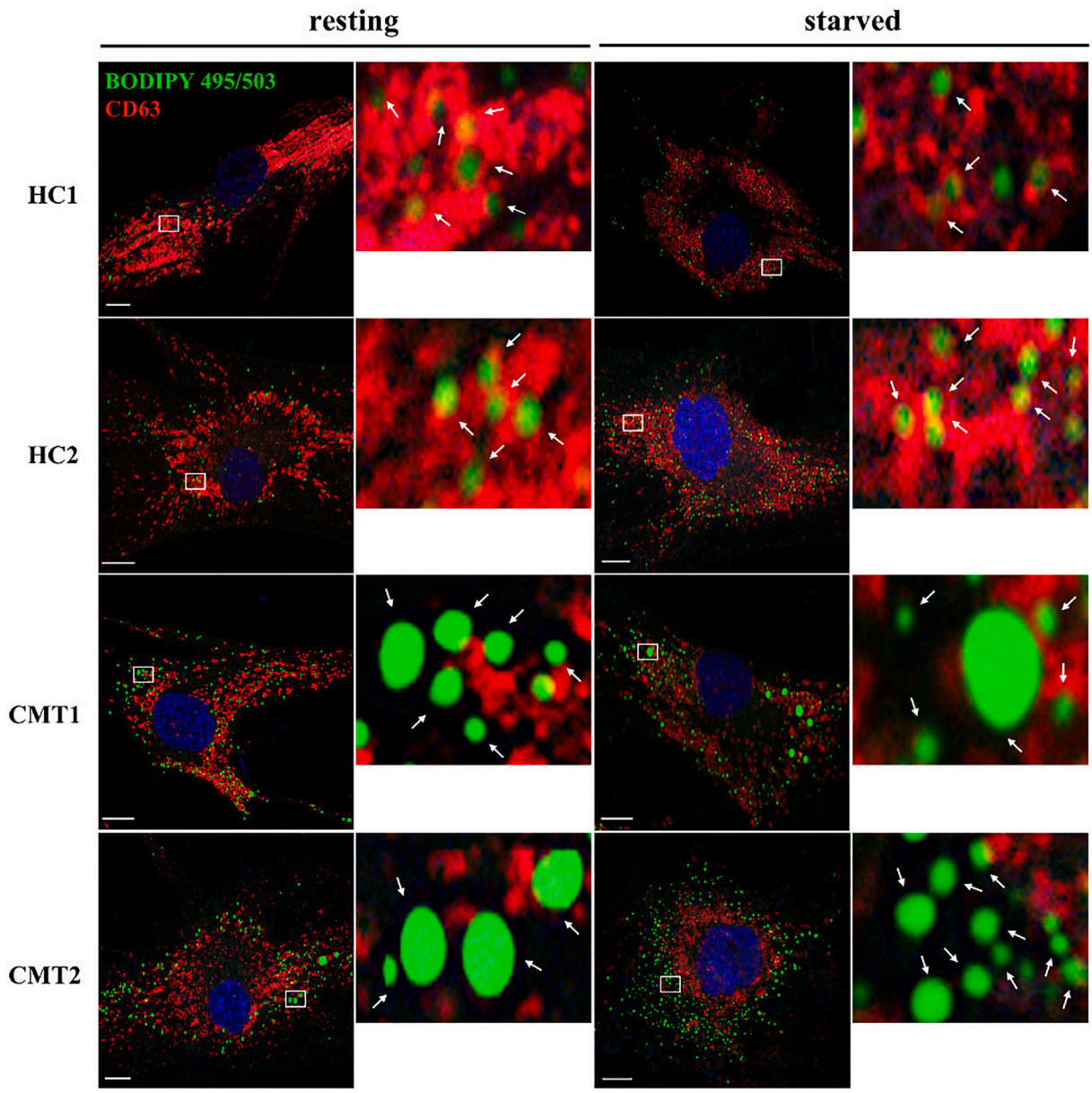

Fig. 8. LD and MVB interaction in HC and CMT2B fibroblasts.
Fibroblasts from healthy individuals (HC1 and HC2) and from patients (CMT1 and CMT2) were cultured with full medium (resting condition) and with EBSS (starved condition) and subjected to immunofluorescence analysis using BODIPY 493/503 to label LDs (green) and anti-CD63 antibody (red). White arrows point to LDs. Nuclei were stained with DAPI (blue). White boxes indicate zoomed areas on the right. Scale bar: 10 μm.

a signaling pathway involving lipogenesis, lipid rafts, AKT and FOXO1 has been also demonstrated [80]. Accordingly, in CMT2B cells we found a significant increase in oleate and in the total MUFA level (Fig. 1). It is interesting to note that variation in SCD1 expression and activity has implications in human pathologies including cancer and neurodegenerative diseases [58,81]. Indeed, studies have documented a progressive increase in MUFA levels and SCD1 expression in the human frontal cortex in patients with bipolar disorder [82] and an increased level of SCD1 was found in Alzheimer's disease subjects [83].

Activated *DN*L in CMT2B cells was linked to SREBP-1 processing, suggesting that lipid-loading in these cells was not a simple passive process. In fact, SREBP-1 is a regulator of a wide array of genes involved in lipid biosynthesis, including those involved in *DN*L (ACC and FAS), TAG synthesis (DGAT), fatty acid desaturation and elongation [62]. SREBP-1 is synthesized as precursors (pSREBP) form at the level of the endoplasmic reticulum. The mature-nuclear (mSREBP) form is generated by proteolytic cleavage after transport to the Golgi.

We found that the precursor but not the mature form of SREBP-1 was significantly decreased in all CMT2B-derived fibroblasts with respect to both controls. Thus, the mSREBP/pSREBP ratio was significantly increased in CMT- compared to HC-derived fibroblasts (Fig. 6a) and this alteration was correlated with the V162M mutation of RAB7, as confirmed by transfection experiments (Fig. 6c). As SREBP-1 mRNA expression levels did not significantly change in CMT2B-derived fibroblasts compared to controls and no effects on SREBP-1 protein levels were observed upon treatment with MG132, a possible explanation for the reduction of the precursor of SREBP-1 could rely either in altered trafficking of the protein or in altered proteolytic activation in CMT2B cells. To this end, it is important to note that cholesterol deprivation is involved in increased translocation of SREBP1 protein from the endoplasmic reticulum to the Golgi apparatus, for the proteolytic activation [84]. Thus, the decreased cholesterol level

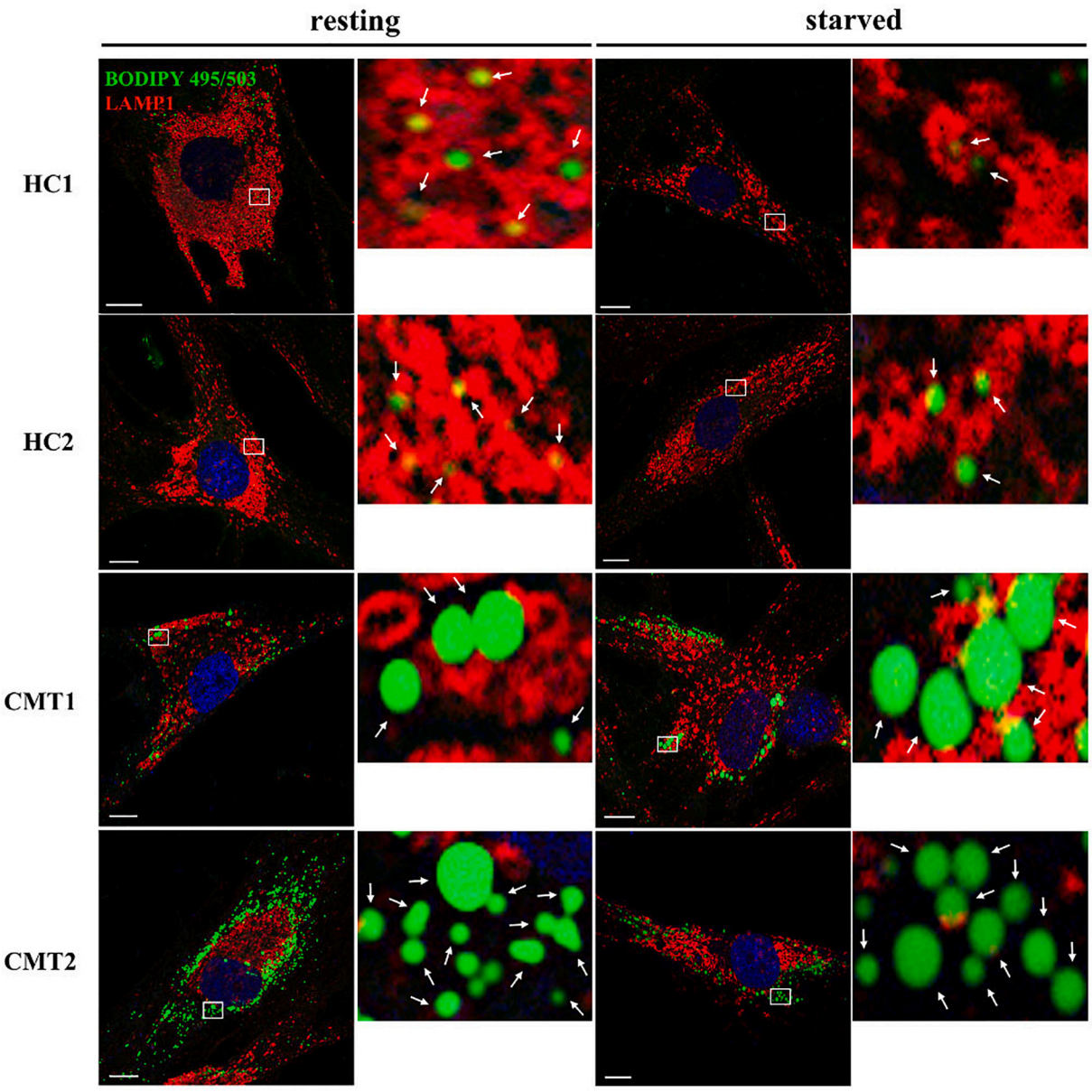

Fig. 9. LD and lysosome interaction in HC and CMT2B fibroblasts.
Fibroblasts from healthy individuals (HC1 and HC2) and from patients (CMT1 and CMT2) were cultured with full medium (resting condition) and with EBSS (starved condition) and subjected to immunofluorescence analysis using BODIPY 493/503 to label LDs (green) and anti-LAMP1 antibody (red). White arrows point to LDs. Nuclei were stained with DAPI (blue). White boxes indicate zoomed areas on the right. Scale bar: 10 μm.

we measured in CMT *vs* controls (Fig. 1b) well correlated with our proposed mechanism.

A recent work reports that oleate is essential for SREBP-1 activity, facilitating its processing and nucleus accumulation where it triggers lipogenic gene expression, including its own expression [85]. Moreover, it has been reported that SREBP-1 cleavage can be facilitated by decreased membrane fluidity and this activation, in turn, induces upregulation of fatty acid synthesis and desaturation [86]. We assume that both mechanisms could be responsible for SREBP-1 activation in CMT2B cells, also considering the increased expression, in CMT2B *vs* HC cells, of Δ-5 and Δ-6 desaturases, key enzymes of PUFA synthesis [87] (Fig. 4). Interestingly, in a work conducted in cultured fibroblasts from Huntington disease patients, a deregulation of fatty acid metabolism and alteration in membrane fluidity has been already demonstrated [88].

In order to establish if the differences in lipid metabolism were related to RAB7 we silenced and overexpressed RAB7 and we expressed the RAB7 V162M mutant in HeLa cells. Importantly, silencing of RAB7 in Hela cells reduced ACC and FAS expression while overexpression of RAB7 and expression of RAB7 V162M mutant increased it. These data allow to correlate the observed changes in lipid metabolism of CMT2B-derived fibroblasts to the $RAB7^{V162M}$ mutation causing CMT2B.

Altogether, these results allow us to hypothesize that, in CMT2B, RAB7 mutations, by altering the autophagic machinery [32], may induce *DN*L and lipid accumulation throughout a SREBP-mediated mechanism. Considering that fatty acids derived from LD hydrolysis represent the main source of mitochondrial β-oxidation [47], impaired lipophagy in CMT2B could induce a deficit in cell energy supply. Finally, toxic effect of lipid accumulation is well documented in neurodegeneration going from neuroinflammation until oxidative stress and mitochondrial dysfunction [89,90]. Interestingly, in mouse model with metabolic syndrome and lipidic dysregulation it was documented Akt2-mediated deficiency in RAB7 protein level and suppression of autophagic flux [91,92]. Thus, we can hypothesize that lipid accumulation

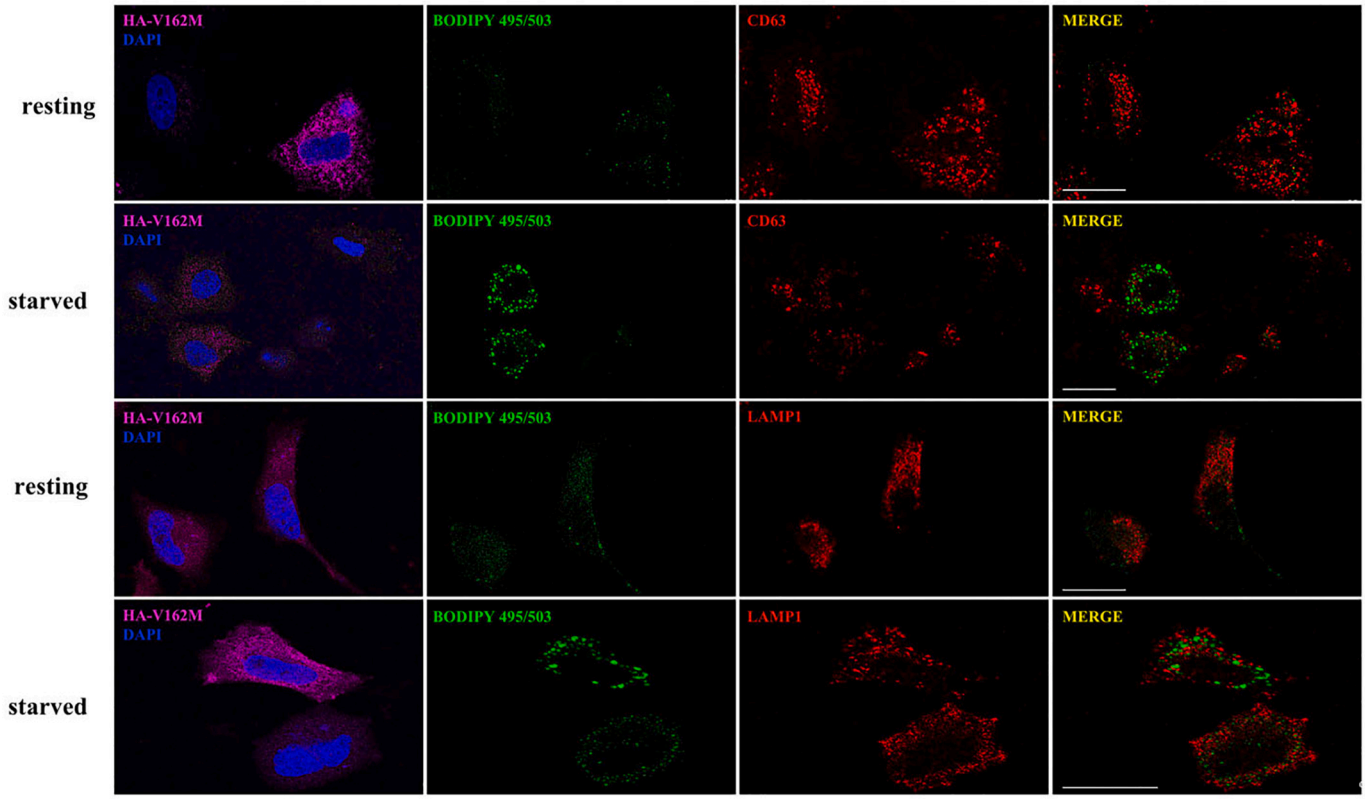

Fig. 10. LD and MVB/lysosome interaction in RAB7 V162M mutant transfected cells.
In HeLa cells expressing RAB7 V162M mutant protein and cultured in full medium (resting condition) or incubated 24 h with EBSS (starved condition), LDs were labeled with BODIPY 493/503 staining (green) and intracellular localization of LDs was evaluated using anti-CD63 and anti-LAMP1 (red) antibodies as indicated. Nuclei are stained with DAPI (blue). Scale bar: 25 μm.

may contribute to autophagic dysfunction in CMT2B generating a vicious circle. If a lipotoxic effect induced by lipid accumulation or an energetic deficit caused by reduced fatty acid mobilization is at the basis of CMT2B-associated neurodegeneration has to be addressed in future studies.

Supplementary data to this article can be found online at https://doi.org/10.1016/j.bbalip.2020.158805.

CRediT authorship contribution statement

Anna Maria Giudetti: Conceptualization, Data curation, Project administration, Writing - original draft, Writing - review & editing. **Flora Guerra:** Conceptualization, Investigation, Data curation, Writing - review & editing. **Serena Longo:** Formal analysis, Writing - review & editing. **Raffaella Beli:** Investigation, Writing - review & editing. **Roberta Romano:** Investigation, Writing - review & editing. **Fiore Manganelli:** Methodology, Writing - review & editing. **Maria Nolano:** Methodology, Writing - review & editing. **Vincenzo Mangini:** Data curation, Writing - review & editing. **Lucio Santoro:** Methodology, Writing - review & editing. **Cecilia Bucci:** Conceptualization, Project administration, Funding acquisition, Writing - original draft, Supervision, Writing - review & editing.

Declaration of competing interest

The authors declare that they have no known competing financial interests or personal relationships that could have appeared to influence the work reported in this paper.

Acknowledgements

The work was supported by Fondazione Telethon (Grant GGP16037 to CB and LS) and by Associazione Italiana per la Ricerca sul Cancro (AIRC, Investigator Grant 2016 N. 19068 to CB). We thank 2HE-PONa3_00334 grant for the Zeiss LSM700 confocal microscope and Fondazione Puglia for the EVOS FL Auto Cell Imaging System.

References

[1] J.M. Vallat, C. Goizet, M. Tazir, P. Couratier, L. Magy, S. Mathis, Classifications of neurogenetic diseases: an increasingly complex problem, Rev. Neurol. (Paris) 172 (2016) 339–349.
[2] G.J. Braathen, Genetic epidemiology of Charcot-Marie-Tooth disease, Acta Neurol. Scand. Suppl. (2012) iv–22.
[3] A.M. Rossor, P.J. Tomaselli, M.M. Reilly, Recent advances in the genetic neuropathies, Curr. Opin. Neurol. 29 (2016) 537–548.
[4] C. Pisciotta, M.E. Shy, Neuropathy, Handb. Clin. Neurol. 148 (2018) 653–665.
[5] D. Pareyson, P. Saveri, C. Pisciotta, New developments in Charcot-Marie-Tooth neuropathy and related diseases, Curr. Opin. Neurol. 30 (2017) 471–480.
[6] C. Bucci, O. Bakke, C. Progida, Charcot-Marie-Tooth disease and intracellular traffic, Prog. Neurobiol. 99 (2012) 191–225.
[7] M.M. Reilly, S.M. Murphy, M. Laurá, Charcot-Marie-Tooth disease, J. Peripher. Nerv. Syst. 16 (2011) 1–14.
[8] B.J. Gentil, L. Cooper, Molecular basis of axonal dysfunction and traffic impairments in CMT, Brain Res. Bull. 88 (2012) 444–453.
[9] H. Houlden, R.H. King, J.R. Muddle, T.T. Warner, M.M. Reilly, R.W. Orrell, L. Ginsberg, A novel RAB7 mutation associated with ulcero-mutilating neuropathy, Ann. Neurol. 56 (2004) 586–590.
[10] K. Verhoeven, P. De Jonghe, K. Coen, N. Verpoorten, M. Auer-Grumbach, J.M. Kwon, D. FitzPatrick, E. Schmedding, E. De Vriendt, A. Jacobs, V. Van Gerwen, K. Wagner, H.P. Hartung, V. Timmerman, Mutations in the small GTP-ase late endosomal protein RAB7 cause Charcot-Marie-Tooth type 2B neuropathy, Am. J. Hum. Genet. 72 (2003) 722–727.
[11] X. Wang, C. Han, W. Liu, P. Wang, X. Zhang, A novel RAB7 mutation in a Chinese family with Charcot-Marie-Tooth type 2B disease, Gene 534 (2014) 431–434.
[12] F. Meggouh, H.M. Bienfait, M.A. Weterman, M. de Visser, F. Baas, Charcot-Marie-Tooth disease due to a de novo mutation of the RAB7 gene, Neurology 67 (2006)

1476–1478.
[13] M. Tazir, T. Hamadouche, S. Nouioua, S. Mathis, J.M. Vallat, Hereditary motor and sensory neuropathies or Charcot-Marie-Tooth diseases: an update, J. Neurol. Sci. 347 (2014) 14–22.
[14] F. Manganelli, C. Pisciotta, V. Provitera, F. Taioli, R. Iodice, A. Topa, G.M. Fabrizi, M. Nolano, L. Santoro, Autonomic nervous system involvement in a new CMT2B family, J. Peripher. Nerv. Syst. 17 (2012) 361–364.
[15] J.P. Luzio, P.R. Pryor, N.A. Bright, Lysosomes: fusion and function, Nat Rev Mol Cell Biol 8 (2007) 622–632.
[16] C. Bucci, P. Thomsen, P. Nicoziani, J. McCarthy, B. van Deurs, Rab7: a key to lysosome biogenesis, Mol. Biol. Cell 11 (2000) 467–480.
[17] S. Jager, C. Bucci, I. Tanida, T. Ueno, E. Kominami, P. Saftig, E.L. Eskelinen, Role for Rab7 in maturation of late autophagic vacuoles, J. Cell Sci. 117 (2004) 4837–4848.
[18] M. Gutierrez, D. Munafó, W. Berón, M. Colombo, Rab7 is required for the normal progression of the autophagic pathway in mammalian cells, J. Cell Sci. 117 (2004) 2687–2697.
[19] R. Harrison, C. Bucci, O. Vieira, T. Schroer, S. Grinstein, Phagosomes fuse with late endosomes and/or lysosomes by extension of membrane protrusions along microtubules: role of Rab7 and RILP, Mol. Cell. Biol. 23 (2003) 6494–6506.
[20] R. Rojas, T. van Vlijmen, G.A. Mardones, Y. Prabhu, A.L. Rojas, S. Mohammed, A.J. Heck, G. Raposo, P. van der Sluijs, J.S. Bonifacino, Regulation of retromer recruitment to endosomes by sequential action of Rab5 and Rab7, J. Cell Biol. 183 (2008) 513–526.
[21] G. Seebohm, N. Strutz-Seebohm, R. Birkin, G. Dell, C. Bucci, M.R. Spinosa, R. Baltaev, A.F. Mack, G. Korniychuk, A. Choudhury, D. Marks, R.E. Pagano, B. Attali, A. Pfeufer, R.S. Kass, M.C. Sanguinetti, J.M. Tavare, F. Lang, Regulation of endocytic recycling of KCNQ1/KCNE1 potassium channels, Circ. Res. 100 (2007) 686–692.
[22] A.L. Edinger, R.M. Cinalli, C.B. Thompson, Rab7 prevents growth factor-independent survival by inhibiting cell-autonomous nutrient transporter expression, Dev. Cell 5 (2003) 571–582.
[23] F. Guerra, C. Bucci, Multiple roles of the small GTPase Rab7, Cells 5 (2016) E34.
[24] K. Deinhardt, S. Salinas, C. Verastegui, R. Watson, D. Worth, S. Hanrahan, C. Bucci, G. Schiavo, Rab5 and Rab7 control endocytic sorting along the axonal retrograde transport pathway, Neuron 52 (2006) 293–305.
[25] S. Saxena, C. Bucci, J. Weis, A. Kruttgen, The small GTPase Rab7 controls the endosomal trafficking and neuritogenic signaling of the nerve growth factor receptor TrkA, J. Neurosci. 25 (2005) 10930–10940.
[26] T. Kawauchi, K. Sekine, M. Shikanai, K. Chihama, K. Tomita, K. Kubo, K. Nakajima, Y. Nabeshima, M. Hoshino, Rab GTPases-dependent endocytic pathways regulate neuronal migration and maturation through N-cadherin trafficking, Neuron 67 (2010) 588–602.
[27] S. BasuRay, S. Mukherjee, E. Romero, M.C. Wilson, A. Wandinger-Ness, Rab7 mutants associated with Charcot-Marie-Tooth disease exhibit enhanced NGF-stimulated signaling, PLoS One 5 (2010) e15351.
[28] B.A. McCray, E. Skordalakes, J.P. Taylor, Disease mutations in Rab7 result in unregulated nucleotide exchange and inappropriate activation, Hum. Mol. Genet. 19 (2010) 1033–1047.
[29] A. De Luca, C. Progida, M.R. Spinosa, P. Alifano, C. Bucci, Characterization of the Rab7K157N mutant protein associated with Charcot-Marie-Tooth type 2B, Biochem. Biophys. Res. Commun. 372 (2008) 283–287.
[30] M.R. Spinosa, C. Progida, A. De Luca, A.M.R. Colucci, P. Alifano, C. Bucci, Functional characterization of Rab7 mutant proteins associated with Charcot-Marie-Tooth type 2B disease, J. Neurosci. 28 (2008) 1640–1648.
[31] L. Cogli, C. Progida, R. Lecci, R. Bramato, A. Krüttgen, C. Bucci, CMT2B-associated Rab7 mutants inhibit neurite outgrowth, Acta Neuropathol. 120 (2010) 491–501.
[32] D. Colecchia, M. Stasi, M. Leonardi, F. Manganelli, M. Nolano, B.M. Veneziani, L. Santoro, E.L. Eskelinen, M. Chiariello, C. Bucci, Alterations of autophagy in the peripheral neuropathy Charcot-Marie-Tooth type 2B, Autophagy 14 (2018) 930–941.
[33] L. Cogli, C. Progida, C.L. Thomas, B. Spencer-Dene, C. Donno, G. Schiavo, C. Bucci, Charcot-Marie-Tooth type 2B disease-causing RAB7A mutant proteins show altered interaction with the neuronal intermediate filament peripherin, Acta Neuropathol. 25 (2013) 257–272.
[34] L. Cogli, C. Progida, R. Bramato, C. Bucci, Vimentin phosphorylation and assembly are regulated by the small GTPase Rab7a, Biochim. Biophys. Acta 1833 (2013) 1283–1293.
[35] J. Yamauchi, T. Torii, S. Kusakawa, A. Sanbe, K. Nakamura, S. Takashima, H. Hamasaki, S. Kawaguchi, Y. Miyamoto, A. Tanoue, The mood stabilizer valproic acid improves defective neurite formation caused by Charcot-Marie-Tooth disease-associated mutant Rab7 through the JNK signaling pathway, J. Neurosci. Res. 88 (2010) 3189–3197.
[36] O.Y. Ponomareva, K.W. Eliceiri, M.C. Halloran, Charcot-Marie-Tooth 2b associated Rab7 mutations cause axon growth and guidance defects during vertebrate sensory neuron development, Neural Dev. 11 (2016) 2.
[37] S. Cherry, E.J. Jin, M.N. Ozel, Z. Lu, E. Agi, D. Wang, W.H. Jung, D. Epstein, I.A. Meinertzhagen, C.C. Chan, P.R. Hiesinger, Charcot-Marie-Tooth 2B mutations in rab7 cause dosage-dependent neurodegeneration due to partial loss of function, Elife 2 (2013) e01064.
[38] K. Janssens, S. Goethals, D. Atkinson, B. Ermanoska, E. Fransen, A. Jordanova, M. Auer-Grumbach, B. Asselbergh, V. Timmerman, Human Rab7 mutation mimics features of Charcot-Marie-Tooth neuropathy type 2B in Drosophila, Neurobiol. Dis. 65 (2014) 211–219.
[39] K. Zhang, R. Fishel, Ben Kenan, Y. Osakada, W. Xu, R.S. Sinit, L. Chen, X. Zhao, J.Y. Chen, B. Cui, C. Wu, Defective axonal transport of Rab7 GTPase results in dysregulated trophic signaling, J Neurosci 33 (2013) 7451–7462.
[40] R. Singh, Autophagy and regulation of lipid metabolism, Results Probl. Cell Differ. 52 (2010) 35–46.
[41] C. Ward, N. Martinez-Lopez, E.G. Otten, B. Carroll, D. Maetzel, R. Singh, S. Sarkar, V.I. Korolchuk, Autophagy, lipophagy and lysosomal lipid storage disorders, Biochim. Biophys. Acta 1861 (2016) 269–284.
[42] E.J. Garcia, J.D. Vevea, L.A. Pon, Lipid droplet autophagy during energy mobilization, lipid homeostasis and protein quality control, Front Biosci (Landmark Ed) 23 (2018) 1552–1563.
[43] N. Martinez-Lopez, R. Singh, Autophagy and lipid droplets in the liver, Annu. Rev. Nutr. 35 (2015) 215–237.
[44] R. Singh, S. Kaushik, Y. Wang, Y. Xiang, I. Novak, M. Komatsu, K. Tanaka, A.M. Cuervo, M.J. Czaja, Autophagy regulates lipid metabolism, Nature 458 (2009) 1131–1135.
[45] J.K. Zehmer, Y. Huang, G. Peng, J. Pu, R.G. Anderson, P. Liu, A role for lipid droplets in inter-membrane lipid traffic, Proteomics 9 (2009) 914–921.
[46] B. Schroeder, R.J. Schulze, S.G. Weller, A.C. Sletten, C.A. Casey, M.A. McNiven, The small GTPase Rab7 as a central regulator of hepatocellular lipophagy, Hepatology 61 (2015) 1896–1907.
[47] K. Liu, M.J. Czaja, Regulation of lipid stores and metabolism by lipophagy, Cell Death Differ. 20 (2013) 3–11.
[48] A. Lizaso, K.T. Tan, Y.H. Lee, β-adrenergic receptor-stimulated lipolysis requires the RAB7-mediated autolysosomal lipid degradation, Autophagy 9 (2013) 1228–1243.
[49] R.J. Schulze, K. Rasineni, S.G. Weller, M.B. Schott, B. Schroeder, C.A. Casey, M.A. McNiven, Ethanol exposure inhibits hepatocyte lipophagy by inactivating the small guanosine triphosphatase Rab7, Hepatol Commun 1 (2017) 140–152.
[50] X. Ding, W. Zhang, T. Zhao, C. Yan, H. Du, Rab7 GTPase controls lipid metabolic signaling in myeloid-derived suppressor cells, Oncotarget 8 (2017) 30123–30137.
[51] A. Garcia-Cazorla, F. Mochel, F. Lamari, J.M. Saudubray, The clinical spectrum of inherited diseases involved in the synthesis and remodeling of complex lipids. A tentative overview, J. Inherit. Metab. Dis. 38 (2015) 19–40.
[52] F. Hullin-Matsuda, T. Taguchi, P. Greimel, T. Kobayashi, Lipid compartmentalization in the endosome system, Semin. Cell Dev. Biol. 31 (2014) 48–56.
[53] A. Nardone, C. Cavaliere, S. Corvigno, G. Limite, S. De Placido, B.M. Veneziani, A banking strategy toward customized therapy in breast cancer, Cell Tissue Bank. 10 (2009) 301–308.
[54] F. Leccia, A. Nardone, S. Corvigno, L.D. Vecchio, S. De Placido, F. Salvatore, B.M. Veneziani, Cytometric and biochemical characterization of human breast cancer cells reveals heterogeneous myoepithelial phenotypes, Cytometry 81 (2012) 960–972.
[55] A. Margiotta, C. Progida, O. Bakke, C. Bucci, Rab7a regulates cell migration through Rac1 and vimentin, Biochim. Biophys. Acta 1864 (2017) 367–381.
[56] F. Guerra, A. Paiano, D. Migoni, G. Girolimetti, A.M. Perrone, P. De Iaco, F.P. Fanizzi, G. Gasparre, C. Bucci, Modulation of RAB7A protein expression determines resistance to cisplatin through late endocytic pathway impairment and extracellular vesicular secretion, Cancers 11 (2019) E52.
[57] B. Fuchs, K. Bresler, J. Schiller, Oxidative changes of lipids monitored by MALDI MS, Chem. Phys. Lipids 164 (2011) 782–795.
[58] A.M. Giudetti, S. De Domenico, A. Ragusa, P. Lunetti, A. Gaballo, J. Franck, P. Simeone, G. Nicolardi, F. De Nuccio, A. Santino, L. Capobianco, P. Lanuti, I. Fournier, M. Salzet, M. Maffia, D. Vergara, A specific lipid metabolic profile is associated with the epithelial mesenchymal transition program, Biochim. Biophys. Acta Mol. Cell Biol. Lipids 1864 (2019) 344–357.
[59] A.M. Giudetti, M. Testini, D. Vergara, P. Priore, F. Damiano, C.A. Gallelli, A. Romano, R. Villani, T. Cassano, L. Siculella, G.V. Gnoni, A. Moles, R. Coccurello, S. Gaetani, Chronic psychosocial defeat differently affects lipid metabolism in liver and white adipose tissue and induces hepatic oxidative stress in mice fed a high-fat diet, FASEB J. 33 (2019) 1428–1439.
[60] D. Vergara, E. Stanca, F. Guerra, P. Priore, A. Gaballo, J. Franck, P. Simeone, M. Trerotola, S. De Domenico, I. Fournier, C. Bucci, M. Salzet, A.M. Giudetti, M. Maffia, Beta-catenin knockdown affects mitochondrial biogenesis and lipid metabolism in breast cancer cells, Front Physiol 8 (2017) 544.
[61] M.J. Wolfgang, M.D. Lane, Control of energy homeostasis: role of enzymes and intermediates of fatty acid metabolism in the central nervous system, Annu. Rev. Nutr. 26 (2006) 23–44.
[62] D. Eberle, B. Hegarty, P. Bossard, P. Ferre, F. Foufelle, SREBP transcription factors: master regulators of lipid homeostasis, Biochimie 86 (2004) 839–848.
[63] A. Bolino, M. Muglia, F.L. Conforti, E. LeGuern, M.A. Salih, D.M. Georgiou, K. Christodoulou, I. Hausmanowa-Petrusewicz, P. Mandich, A. Schenone, A. Gambardella, F. Bono, A. Quattrone, M. Devoto, A.P. Monaco, Charcot-Marie-Tooth type 4B is caused by mutations in the gene encoding myotubularin-related protein-2, Nat. Genet. 25 (2000) 17–19.
[64] J. Senderek, C. Bergmann, S. Weber, U.P. Ketelsen, H. Schorle, S. Rudnik-Schoneborn, R. Buttner, E. Buchheim, K. Zerres, Mutation of the SBF2 gene, encoding a novel member of the myotubularin family, in Charcot–Marie–Tooth neuropathy type 4B2/11p15, Hum. Mol. Genet. 12 (2003) 349–356.
[65] C.Y. Chow, Y. Zhang, J.J. Dowling, N. Jin, M. Adamska, K. Shiga, K. Szigeti, M.E. Shy, J. Li, X. Zhang, J.R. Lupski, L.S. Weisman, M.H. Meisler, Mutation of Fig 4 causes neurodegeneration in the pale tremor mouse and patients with CMT4J, Nature 448 (2007) 68–72.
[66] I. Vaccari, A. Carbone, S.C. Previtali, Y.A. Mironova, V. Alberizzi, R. Noseda, C. Rivellini, F. Bianchi, U. Del Carro, M. D'Antonio, G.M. Lenk, L. Wrabetz, R.J. Giger, M.H. Meisler, A. Bolino, Loss of Fig 4 in both Schwann cells and motor neurons contributes to CMT4J neuropathy, Hum. Mol. Genet. 24 (2015) 383–396.
[67] L. Kalaydjieva, D. Gresham, R. Gooding, L. Heather, F. Baas, R. de Jonge, K. Blechschmidt, D. Angelicheva, D. Chandler, P. Worsley, A. Rosenthal, R.H. King,

P.K. Thomas, N-myc downstream-regulated gene 1 is mutated in hereditary motor and sensory neuropathy-Lom, Am. J. Hum. Genet. 67 (2000) 47–58.
[68] V. Pietiainen, B. Vassilev, T. Blom, W. Wang, J. Nelson, R. Bittman, N. Back, N. Zelcer, E. Ikonen, NDRG1 functions in LDL receptor trafficking by regulating endosomal recycling and degradation, J. Cell Sci. 126 (2013) 3961–3971.
[69] Y.B. Hong, J. Kang, J.H. Kim, J. Lee, G. Kwak, Y.S. Hyun, S.H. Nam, H.D. Hong, Y.R. Choi, S.C. Jung, H. Koo, J.E. Lee, B.O. Choi, K.W. Chung, DGAT2 mutation in a family with autosomal-dominant early-onset axonal Charcot-Marie-Tooth disease, Hum. Mutat. 37 (2016) 473–480.
[70] W.L. Miller, Disorders in the initial steps of steroid hormone synthesis, J. Steroid Biochem. Mol. Biol. 165 (2017) 18–37.
[71] W.C. Man, M. Miyazaki, K. Chu, J. Ntambi, Colocalization of SCD1 and DGAT2: implying preference for endogenous monounsaturated fatty acids in triglyceride synthesis, J. Lipid Res. 47 (2006) 1928–1939.
[72] T.C. Walther, J. Chung, R.V. Farese Jr., Lipid droplet biogenesis, Annu. Rev. Cell Dev. Biol. 33 (2017) 491–510.
[73] T.C. Walther, R.V. Farese Jr., Lipid droplets and cellular lipid metabolism, Annu. Rev. Biochem. 81 (2012) 687–714.
[74] R. Singh, A.M. Cuervo, Lipophagy: connecting autophagy and lipid metabolism, Int J Cell Biol 2012 (2012) 282041.
[75] L. Kuerschner, C. Moessinger, C. Thiele, Imaging of lipid biosynthesis: how a neutral lipid enters lipid droplets, Traffic 9 (2008) 338–352.
[76] P.J. McFie, S.L. Banman, S.J. Stone, Diacylglycerol acyltransferase-2 contains a c-terminal sequence that interacts with lipid droplets, Biochim. Biophys. Acta Mol. Cell Biol. Lipids 1863 (2018) 1068–1081.
[77] J.M. Collins, M.J. Neville, M.B. Hoppa, K.N. Frayn, De novo lipogenesis and stearoyl-CoA desaturase are coordinately regulated in the human adipocyte and protect against palmitate-induced cell injury, J. Biol. Chem. 285 (2010) 6044–6052.
[78] D.I. Sinner, G.J. Kim, G.C. Henderson, R.A. Igal, StearoylCoA desaturase-5: a novel regulator of neuronal cell proliferation and differentiation, PLoS One 7 (2012) e39787.
[79] M.F. Chong, L. Hodson, A.S. Bickerton, R. Roberts, M. Neville, F. Karpe, K.N. Frayn, B.A. Fielding, Parallel activation of de novo lipogenesis and stearoyl-CoA desaturase activity after 3 d of high-carbohydrate feeding, Am. J. Clin. Nutr. 87 (2008) 817–823.
[80] S.H. Tan, G. Shui, J. Zhou, Y. Shi, J. Huang, D. Xia, M.R. Wenk, H.M. Shen, Critical role of SCD1 in autophagy regulation via lipogenesis and lipid rafts-coupled AKT-FOXO1 signaling pathway, Autophagy 10 (2014) 226–242.
[81] S.B. Narayan, D. Rakheja, L. Tan, J.V. Pastor, M.J. Bennett, CLN3P, the Batten's disease protein, is a novel palmitoyl-protein Delta-9 desaturase, Ann. Neurol. 60 (2006) 570–577.
[82] R.K. McNamara, R. Jandacek, T. Rider, P. Tso, K.E. Stanford, C.G. Hahn, N.M. Richtand, Deficits in docosahexaenoic acid and associated elevations in the metabolism of arachidonic acid and saturated fatty acids in the postmortem orbitofrontal cortex of patients with bipolar disorder, Psychiatry Res. 160 (2008) 285–299.
[83] G. Astarita, K.M. Jung, V. Vasilevko, N.V. Dipatrizio, S.K. Martin, D.H. Cribbs, E. Head, C.W. Cotman, D. Piomelli, Elevated stearoyl-CoA desaturase in brains of patients with Alzheimer's disease, PLoS One 6 (2011) e24777.
[84] R. Bertolio, F. Napoletano, M. Mano, S. Maurer-Stroh, M. Fantuz, A. Zannini, S. Bicciato, G. Sorrentino, G. Del Sal, Sterol regulatory element binding protein 1 couples mechanical cues and lipid metabolism, Nat. Commun. 10 (2019) 1326.
[85] M.A. Lounis, K.F. Bergeron, M.S. Burhans, J.M. Ntambi, C. Mounier, Oleate activates SREBP-1 signaling activity in SCD1-deficient hepatocytes, Am. J. Physiol. Endocrinol. Metab. 313 (2017) E710–E720.
[86] R.M. Hagen, S. Rodriguez-Cuenca, A. Vidal-Puig, An allostatic control of membrane lipid composition by SREBP1, FEBS Lett. 584 (2010) 2689–2698.
[87] F. Tosi, F. Sartori, P. Guarini, O. Olivieri, N. Martinelli, Delta-5 and delta-6 desaturases: crucial enzymes in polyunsaturated fatty acid-related pathways with pleiotropic influences in health and disease, Adv. Exp. Med. Biol. 824 (2014) 61–81.
[88] F. Schroeder, I.E. Goetz, E. Roberts, Membrane anomalies in Huntington's disease fibroblasts, J. Neurochem. 43 (1984) 526–539.
[89] M.A. Welte, Expanding roles for lipid droplets, Curr. Biol. 25 (2015) R470–R481.
[90] J. Kang, S. Rivest, Lipid metabolism and neuroinflammation in Alzheimer's disease: a role for liver X receptors, Endocr. Rev. 33 (2012) 715–746.
[91] B. Jaishy, E.D. Abel, Lipids, lysosomes, and autophagy, J. Lipid Res. 57 (2016) 1619–1635.
[92] X. Xu, Y. Hua, S. Nair, Y. Zhang, J. Ren, Akt2 knockout preserves cardiac function in high-fat diet-induced obesity by rescuing cardiac autophagosome maturation, J. Mol. Cell Biol. 5 (2013) 61–63.